HAL open science

Time minimal saturation of a pair of spins and application in magnetic resonance imaging

Bernard Bonnard, Olivier Cots, Jérémy Rouot, Thibaut Verron

To cite this version:

Bernard Bonnard, Olivier Cots, Jérémy Rouot, Thibaut Verron. Time minimal saturation of a pair of spins and application in magnetic resonance imaging. Mathematical Control and Related Fields, 2020, 10 (1), pp.47-88. 10.3934/mcrf.2019029 . hal-01779377v3

HAL Id: hal-01779377

https://inria.hal.science/hal-01779377v3

Submitted on 4 Jan 2019

HAL is a multi-disciplinary open access archive for the deposit and dissemination of scientific research documents, whether they are published or not. The documents may come from teaching and research institutions in France or abroad, or from public or private research centers.

L'archive ouverte pluridisciplinaire **HAL**, est destinée au dépôt et à la diffusion de documents scientifiques de niveau recherche, publiés ou non, émanant des établissements d'enseignement et de recherche français ou étrangers, des laboratoires publics ou privés.

Manuscript submitted to
AIMS' Journals
Volume **X**, Number **0X**, XX **200X**

doi:10.3934/xx.xx.xx.xx

pp. **X–XX**

TIME MINIMAL SATURATION OF A PAIR OF SPINS AND APPLICATION IN MAGNETIC RESONANCE IMAGING

Bernard Bonnard

Institut de Mathématiques de Bourgogne, Université de Bourgogne,
9 avenue Alain Savary, 21078 Dijon, France.
And INRIA, 2004 route des Lucioles F-06902, Sophia Antipolis, France.

Olivier Cots

Toulouse Univ., INP-ENSEEIHT-IRIT,
UMR CNRS 5505, 2 rue Camichel, 31071 Toulouse, France.

Jérémy Rouot*

Institut de Mathématiques de Bourgogne, Université de Bourgogne,
9 avenue Alain Savary, 21078 Dijon, France.
And EPF:École d'Ingénieur-e-s, 2 Rue F Sastre,
10430 Rosières-prés-Troyes, France.

Thibaut Verron

Institute for Algebra, Johannes Kepler University,
4040 Linz, Austria.

(Communicated by the associate editor name)

Abstract. In this article, we analyze the time minimal control for the saturation of a pair of spins of the same species but with inhomogeneities of the applied RF-magnetic field, in relation with the contrast problem in Magnetic Resonance Imaging. We make a complete analysis based on geometric control to classify the optimal syntheses in the single spin case to pave the road to analyze the case of two spins. The `Bocop` software is used to determine local minimizers for physical test cases and Linear Matrix Inequalities approach is applied to estimate the global optimal value and validate the previous computations. This is complemented by numerical computations combining shooting and continuation methods implemented in the `HamPath` software to analyze the structure of the time minimal solution with respect to the set of parameters of the species. Symbolic computations techniques are used to handle the singularity analysis.

2010 *Mathematics Subject Classification.* AMS Subject Classification: 49K15, 49M15, 81Q93, 14Q20.

Key words and phrases. Geometric optimal control; Contrast imaging in NMR; Direct method; Shooting and continuation techniques; Moment optimization; Gröbner basis.

The first author is partially supported by the ANR Project - DFG Explosys (Grant No. ANR-14-CE35-0013-01;GL203/9-1), the fourth author is supported by the Austrian FWF grant F5004, and the four authors are supported by the FMJH PGMO and from the support of EDF, Thales and Orange.

* Corresponding author.

1. **Introduction.** In Nuclear Magnetic Resonance (NMR) *saturating* one chemical species consists of driving the magnetization vector representing the state to zero. In Magnetic Resonance Imaging (MRI) a challenging problem is to maximize the *contrast* between two observed species (for instance, healthy tissues and tumors) saturating one species. Optimal control techniques in NMR were introduced in this domain in the eighties [18] and were developed in MRI very recently under the impulse of S. Glaser using advanced analytical and numerical techniques. This gave rise to a series of articles [23, 24, 10, 8, 37] starting from the ideal case where only a pair of spins is considered to the optimal control of an *ensemble* of pairs of spins corresponding to the experimental situation, whose aim is to construct a *robust* control to deal with the so-called B_0 and B_1 inhomogeneities associated to perturbations of the applied magnetic fields. The starting point of this study being the explicit computation of the time minimal solution of the saturation of a single spin [29], showing in particular that the standard so-called inversion sequence applied in practise is not optimal in many physical cases. Additional pulses have to be used and correspond to the so-called singular control whose importance is well known in geometric optimal control [5]. More precisely the computation of the optimal solution relies on an intense research activity of the end of the eighties about the calculation of a closed loop time minimal solution for a $\mathcal{C}^\omega$-planar single input control system in a neighbourhood of a given point, taking into account the Lie algebraic structure of the system at this point [13, 36, 34, 35].

A first contribution of this article is to make a complete classification of the time minimal synthesis to saturate a single spin, taking into account the relaxation parameters of the species and the maximal amplitude of the applied RF (B_1) field, hence completing [23]. The next step, studied in details in this article, is to extend this analysis to the case of two spins. For simplicity we consider the case associated to the so-called B_1-inhomogeneity that is a variation of the applied RF field. Still, the analysis is very complex and we present a combination of algebraic and geometric method introduced in [5] and adapted numerical schemes implemented in specific softwares: `Bocop` [3], `HamPath` [16], `GloptiPoly` [20] to give a neat analysis of the problem, generalizing the case of a single spin.

This article is organized as follows. In section 2, we present the mathematical model, that is the Bloch equations [27] and we discuss the underlying optimal control problem in MRI, that is the contrast problem [24] with B_0 and B_1 inhomogeneities, to introduce the time minimal saturation of a pair of spins, that we analyze in this article. The seminal result in optimal control theory is the Maximum Principle [32] which is recalled to select extremal curves candidates as minimizers. The extremal controls split into bang controls and the so-called singular controls whose role in the time minimal problem is recalled [7]. A preliminary study concerning the case of a single spin is presented in details in section 3 using geometric control theory techniques. This leads to a complete classification of the optimal syntheses to steer the system from the North Pole to any reachable state. Thanks to the symmetry of revolution it is reduced to a time minimal control problem for a single-input 2D-system. All the fine results of the geometric theory [14, 36] are used to provide a complete classification depending upon the physical parameters and completing [23]. The next steps in sections 4 and 5 are to extend this analysis to a pair of spins of the same species with B_1-inhomogeneities, and numerical methods, presented in sections 6 and 7, are used to complete this analysis. Section 4 leads to identify a simplified case corresponding to the so-called water case, important in practice and

which is a generalization of the standard inversion sequence for a single spin. This case is important to analyze the general case, using homotopy methods. In section 5, we discuss the theoretical complexity of the procedure. The crucial point is to analyze the singular trajectories associated with a $4D$-Hamiltonian flow, with constraints and many singularities. They are computed using symbolic computations, extending techniques from [6, 12]. In section 6, the direct methods implemented in the `Bocop` code are applied to analyze some physical cases: Deoxygenated and Oxygenated blood case, Cerebrospinal fluid and Water case. Then, global optimality is analyzed using LMI methods [25]. In section 7, the problem is studied using multiple shooting methods implemented in the `HamPath` software and completed by numerical continuations (available in the software) to compute the optimal solutions for a continuous set of physical relaxation parameters. This numerical investigation, based on homotopy, reveals the existence of path of zeros that we have to compare to determine the global optimum. This was already observed in the contrast problem, see [9].

2. Multi-saturation: general concepts and results.

2.1. **The model.** We consider an ensemble of spin-1/2 particules, excited by a radio-frequency (RF) field which is ideally assumed homogeneous, each spin of this ensemble being described by the magnetization vector $M := (M_x, M_y, M_z)$ whose dynamics is governed in a specific rotating frame by the *Bloch equation* [27]:

$$\begin{aligned}
\dot{M}_x(t) &= -\frac{M_x(t)}{T_2} + \omega_y(t)\, M_z(t),\\
\dot{M}_y(t) &= -\frac{M_y(t)}{T_2} - \omega_x(t)\, M_z(t),\\
\dot{M}_z(t) &= \frac{M_0 - M_z(t)}{T_1} - \omega_y(t)\, M_x(t) + \omega_x(t)\, M_y(t),
\end{aligned}$$

where T_1, T_2 are respectively the *longitudinal, transversal relaxation constants*, M_0 is the *thermal equilibrium* and $\omega := (\omega_x, \omega_y)$ is the *control* corresponding to the applied RF-magnetic field, with $\omega_{\max}$ the maximal amplitude of the control, *i.e.* $\omega_x^2 + \omega_y^2 \leq \omega_{\max}^2$. Table 1 gives a list of longitudinal and transversal relaxation constants for the main practical cases. Up to a renormalization of M introducing $(x, y, z) := (M_x, M_y, M_z)/M_0$ and a time reparameterization, the dynamics take the form:

$$\begin{aligned}
\dot{x}(t) &= -\Gamma\, x(t) + u_y(t)\, z(t),\\
\dot{y}(t) &= -\Gamma\, y(t) - u_x(t)\, z(t),\\
\dot{z}(t) &= \gamma\,(1 - z(t)) - u_y(t)\, x(t) + u_x(t)\, y(t).
\end{aligned}$$

In the relevant physical cases, one has $0 < \gamma \leq 2\Gamma$ and the Bloch ball: $x^2+y^2+z^2 \leq 1$, is invariant for the dynamics. Thanks to the reparameterization, one can assume that the control is bounded by $u_x^2 + u_y^2 \leq 1$. In this case, the relations between the parameters (γ, Γ) and $(T_1, T_2, \omega_{\max})$ are the following:

$$\gamma = \frac{1}{T_1\, \omega_{\max}}, \quad \Gamma = \frac{1}{T_2\, \omega_{\max}}. \tag{1}$$

The system admits a symmetry of revolution around the z-axis, which allows us to set $u_y = 0$ and to restrict each spin system to a single-input control system in the

Name	T_1	T_2	$\frac{T_2}{T_1} = \frac{\gamma}{\Gamma}$	$\theta = \text{atan}(\frac{\gamma}{\Gamma})$
Water	2.5	2.5	1.0	0.7854
Fat	0.2	0.1	0.5	0.4636
Cerebrospinal Fluid	2.0	0.3	0.15	0.1489
Oxygenated blood	1.35	0.2	0.1481	0.1471
White cerebral matter	0.78	0.09	0.1154	0.1148
Gray cerebral matter	0.92	0.1	0.1087	0.1083
Brain	1.062	0.052	0.0490	0.0489
Deoxygenated blood	1.35	0.05	0.0370	0.0370
Parietal muscle	1.2	0.029	0.0242	0.0242

TABLE 1. Matter name with relaxation times in seconds, ratio T_2/T_1 and value $\theta = \text{atan}(\gamma/\Gamma)$.

trace of the Bloch ball on the plane (y, z). The system then takes the form:

$$\begin{aligned} \dot{y}(t) &= -\Gamma\, y(t) - u(t)\, z(t), \\ \dot{z}(t) &= \gamma\,(1 - z(t)) + u(t)\, y(t), \end{aligned} \tag{2}$$

with $u = u_x$, $|u| \leq 1$.

The *problem of saturation* associated to the contrast problem by saturation in MRI is to steer from the North Pole $N := (0, 1)$ to the origin $O := (0, 0)$ one of the two species to be distinguished. In the contrast problem with RF-inhomogeneities, which is due to the spatial position of the species in the image, one has to consider an ensemble of pair of spins, such as for each system, the dynamics is perturbed. This perturbation is modeled as a rescaling of the maximal amplitude perceived by the spin. Restricting again to the sub-problem of saturation of one species, and considering only an ensemble of two pairs of spins, this leads to consider the case of a couple of systems (2) with the same parameters (γ, Γ) but with a distortion in the maximal amplitude, that is:

$$\begin{cases} \dot{y}_1 = -\Gamma\, y_1 - u\, z_1, \\ \dot{z}_1 = \gamma\,(1 - z_1) + u\, y_1, \end{cases} \qquad \begin{cases} \dot{y}_2 = -\Gamma\, y_2 - (1 - \varepsilon)\, u\, z_2, \\ \dot{z}_2 = \gamma\,(1 - z_2) + (1 - \varepsilon)\, u\, y_2, \end{cases}$$

where $|u| \leq 1$, with $q_1 := (y_1, z_1)$, $q_2 := (y_2, z_2)$ denote the coordinates of spin 1 and spin 2 and $(1-\varepsilon)$, $\varepsilon > 0$ small, is the *rescaling factor* of the control maximal amplitude. Hence, the *saturation problem of a pair of spins* consists into a simultaneous steering of the couple from $q_1(0) = q_2(0) = N$ to the center $q_1(t_f) = q_2(t_f) = O$, where t_f is the transfer time. The optimal control problem that we shall analyze is the *time minimal saturation problem*, *i.e.* we aim to minimize the transfer time t_f.

2.2. **Maximum principle and singular extremals.**

2.2.1. *Preliminaries.* In this section, we consider a single-input control system: $\frac{\mathrm{d}q}{\mathrm{d}t} = F + u\,G$, where F, G are $\mathcal{C}^\omega$ vector fields defined on an open subset $V \subset \mathbb{R}^n$ and the control u is a bounded measurable mapping defined on $[0\,,T_u]$ and valued in $|u| \leq 1$. For fixed q_0 and $T > 0$, the *extremity mapping* is the map $E\colon u \in L^\infty([0\,,T]) \mapsto E(u) = q(T, q_0, u)$, where $q(\cdot, q_0, u)$ is the solution of the system with $q(0, q_0, u) = q_0$. A control $u \in L^\infty([0\,,T])$ is called *singular* if the extremity mapping is not of full rank and the corresponding trajectory is called singular on $[0\,,T]$. We have the following relations with the time minimal control problem [32].

Proposition 1. *Consider the time minimal control problem for the single-input control system:* $\frac{\mathrm{d}q}{\mathrm{d}t} = F + u\,G$, $|u| \leq 1$. *If* $u(\cdot)$, *with corresponding trajectory* $q(\cdot)$, *is solution, then there exists* $p(\cdot)$, $t \mapsto p(t) \in \mathbb{R}^n \setminus \{0_{\mathbb{R}^n}\}$, *such that the following equations are satisfied for the triplet* $(q(\cdot), p(\cdot), u(\cdot))$*:*

$$\dot{q} = \frac{\partial H}{\partial p}, \quad \dot{p} = -\frac{\partial H}{\partial q} \quad a.e. \tag{3}$$

$$H(q(t), p(t), u(t)) = \max_{|v|\leq 1} H(q(t), p(t), v) \quad a.e. \tag{4}$$

where p *is the adjoint vector and* $H(q, p, u) := p\cdot(F + u\,G)$ *is the pseudo-Hamiltonian. Moreover,* $M(q, p) := \max_{|v|\leq 1} H(q, p, v)$ *is constant along* $(q(\cdot), p(\cdot))$ *and non-negative.*

Definition 2.1. A triplet $(q(\cdot), p(\cdot), u(\cdot))$ solution of (3) and (4) is called an *extremal*. It is called *regular* if $u(t) = \mathrm{sign}(p(t) \cdot G(q(t)))$ *a.e.* and *bang-bang* if it is regular and the number of switchings of $u(\cdot)$ is finite. An extremal is called *singular* if $p(\cdot) \cdot G(q(\cdot)) = 0$ everywhere. We denote by σ_+, σ_- and σ_s respectively bang with $u = +1$, $u = -1$ and singular extremals. Extremals satisfying the boundary conditions are called *BC-extremals*.

Proposition 2. *If the control* $u(\cdot)$ *is singular on* $[0\,,T]$ *(for the extremity mapping), with* $q(\cdot)$ *the associated trajectory, then there exists* $p(\cdot)$ *such that* $(q(\cdot), p(\cdot), u(\cdot))$ *is a singular extremal.*

2.2.2. *Computation of singular trajectories.* The *Lie bracket* of two $\mathcal{C}^\omega$ vector fields X, Y on V is computed with the convention:

$$[X, Y](q) := \frac{\partial Y}{\partial q}(q)\,X(q) - \frac{\partial X}{\partial q}(q)\,Y(q),$$

and denoting H_X, H_Y the Hamiltonian lifts: $H_X(z) := p \cdot X(q)$, $H_Y(z) := p \cdot Y(q)$, with $z := (q, p) \in V \times \mathbb{R}^n$, the *Poisson bracket* reads:

$$\{H_X, H_Y\} := \mathrm{d}H_Y \cdot \overrightarrow{H}_X = p \cdot [X, Y](q),$$

where $\overrightarrow{H}_X := \frac{\partial H}{\partial p}\frac{\partial}{\partial q} - \frac{\partial H}{\partial q}\frac{\partial}{\partial p}$. Differentiating twice $p(\cdot) \cdot G(q(\cdot))$ with respect to the time t, one gets:

Proposition 3. *Singular extremals* $(z(\cdot), u(\cdot))$ *are solutions of the following equations:*

$$H_G(z(t)) = \{H_F, H_G\}(z(t)) = 0,$$
$$\{H_F, \{H_F, H_G\}\}(z(t)) + u(t)\,\{H_G, \{H_F, H_G\}\}(z(t)) = 0.$$

If $\{H_G, \{H_F, H_G\}\} \neq 0$ along the extremal, then the singular control is called of minimal order and it is given by the dynamic feedback:

$$u_s(z(t)) := -\frac{\{H_F, \{H_F, H_G\}\}(z(t))}{\{H_G, \{H_F, H_G\}\}(z(t))}.$$

From the above proposition one gets:

Corollary 1. *If $u(\cdot) = 0$ is a singular control on $[0\,, T]$ then one has:*

$$\mathrm{ad}^k\, H_F \cdot H_G(z(t)) = p(\cdot) \cdot (\mathrm{ad}^k\, F \cdot G(q(t))), \quad \forall\, k \geq 0,$$

with $\mathrm{ad}\, F \cdot G := [F, G]$, $\mathrm{ad}\, H_F \cdot H_G := \{H_F, H_G\}$.

Corollary 2. *Up to the reparameterization* $\mathrm{d}s := \mathrm{d}t/\{H_G, \{H_F, H_G\}\}(z(t))$, *singular extremals of minimal order are solutions of the analytic differential equation* $\frac{\mathrm{d}z}{\mathrm{d}s} = X(z)$, *with*

$$\begin{aligned} X :=& \Big(\{H_G, \{H_F, H_G\}\}\, F - \{H_F, \{H_F, H_G\}\}\, G\Big) \frac{\partial}{\partial q} \\ &- \Big(\{H_G, \{H_F, H_G\}\} \frac{\partial F}{\partial q} - \{H_F, \{H_F, H_G\}\} \frac{\partial G}{\partial q}\Big) \frac{\partial}{\partial p}, \end{aligned}$$

with two constraints $H_G(z) = \{H_F, H_G\}(z) = 0$.

2.2.3. *Classification of singular extremals and time optimality properties.* In this section we recall results from [13] about singular extremals. We consider the C^ω-single input control system relaxing the control bound $|u| \leq 1$:

$$\dot{q} = F(q) + u\, G(q), \quad u \in \mathbb{R}.$$

Let $\gamma(t) := (q(t), p(t)),\ t \in [0, T]$ be a reference singular extremal of minimal order and assume that $t \mapsto q(t)$ is one-to-one. Assuming F, G not collinear along $q(\cdot)$ one can assume that $q(\cdot)$ is a singular trajectory associated to $u_s \equiv 0$. The first order Pontryagin cone $K(t)$ is the subspace of codimension ≥ 1 generated by the vectors $\mathrm{ad}^k\, F \cdot G(q(t)),\ k \geq 0$. We introduce the following generic assumptions

(H1) $\forall t \in [0, T],\ \mathrm{ad}^2\, G \cdot F(q(t)) \notin K(t)$;
(H2) $\forall t$, $K(t)$ is exactly of codimension one and generated by the vectors $\{\mathrm{ad}^k\, G \cdot F(q(t));\ k = 0, \ldots n-2\}$;
(H3) If $n \geq 3$, $\forall t \in [0, T]$, $F(q(t)) \notin \mathrm{span}\{\mathrm{ad}^k\, F \cdot G(q(t));\ k = 0, \ldots, n-3\}$.

Under these assumptions, the problem is *normal* that is the adjoint vector $p(\cdot)$ associated to $q(\cdot)$ is unique up to a factor and $\forall t \in [0, T],\ p(t)$ is orthogonal to $K(t)$. Orienting $p(\cdot)$ using the convention of the Maximum Principle: $\langle p(t), F(q(t))\rangle \geq 0$, the singular trajectory is called

- *Hyperbolic* if $\langle p(t), \mathrm{ad}^2\, G \cdot F(q(t)\rangle > 0$;
- *Elliptic* if $\langle p(t), \mathrm{ad}^2\, G \cdot F(q(t)\rangle < 0$;
- *Exceptional* if $\langle p(t),\ F(q(t))\rangle = 0$.

Note that the condition $\langle p(t), \mathrm{ad}^2\ G \cdot F(q(t))\rangle \geq 0$ amounts to the *generalized Legendre-Clebsch* condition

$$\frac{\partial}{\partial u} \frac{\mathrm{d}^2}{\mathrm{d}t^2} \frac{\partial H}{\partial u}(\gamma(t)) \geq 0$$

and according to the *higher-order maximum principle* [21], this condition is a necessary (small) time minimization condition. The key result is the following.

Theorem 2.2. *Under assumptions* (H_1), (H_2) *and* (H_3) *an exceptional or hyperbolic (respectively elliptic) trajectory is time minimizing (respectively time maximizing) on* $[0, T]$ *with respect to all trajectories contained in a* C^0*-neighbourhood of* $q(\cdot)$ *if* $T < t_{1c}$*, where* $t_{1c} > 0$ *is called the first conjugate time along* $q(\cdot)$*.*

Algorithms to compute the fist conjugate times are described in [4] and are implemented in the `HamPath` code. This gives a complete characterization of the time minimality status of the singular extremals under (generic) assumptions, when the control bound $|u| \leq 1$ is relaxed. To complete the analysis, we have to check if the singular control satisfies the constraint $|u_s| \leq 1$, that is if the *singular arc is admissible*. If $|u_s| = 1$ then we say that the control *saturates* the constraint. If $|u_s| > 1$, then the singular control is not admissible and with some abuse, we shall use the terminology *parabolic arc* for the corresponding trajectory. See [22] for this terminology.

3. **Mono-saturation: optimal syntheses.** We refer to [35, 14] for the standard concepts of *regular synthesis* used in our analysis. We have two cases:

- case 1: fix the initial point to be the North Pole $N = (0, 1)$;
- case 2: fix the final point to be the center $O = (0, 0)$.

We consider the first case to complete the results from [10], giving the optimal syntheses for all authorized values of the relaxation parameters. The optimal control problem we consider here may be written in the following form:

$$v(q_f) := \inf_{u \in \mathcal{U}} T_u, \quad \text{s.t.} \quad q(T_u, q_0, u) = q_f,$$

where $\mathcal{U} = \{u \colon [0\,, \infty) \to [-1\,, 1] \mid u(\cdot) \text{ measurable}\}$ is the set of admissible controls and where $q(T, q_0, u)$ is the solution at time T of the system (2) with control u and initial condition q_0, which is in this case the North Pole, that is $q_0 := (0, 1) = N$. For a given reachable final condition q_f, one can denote by $u^*(\cdot, q_f)$ the optimal control (if it is unique). The goal is thus to give for any reachable state q_f the value function at q_f, that is $v(q_f)$, together with the optimal control law $u^*(\cdot, q_f)$. This analysis exhibits three different optimal syntheses depending on the relaxation parameters (γ, Γ).

3.1. **Lie brackets computations.** The system (2) is written as:

$$\frac{\mathrm{d}q}{\mathrm{d}t} = F(q) + u\, G(q), \quad |u| \leq 1,$$

with

$$F(q) := -\Gamma\, y \frac{\partial}{\partial y} + \gamma\,(1 - z) \frac{\partial}{\partial z}, \quad G(q) := -z \frac{\partial}{\partial y} + y \frac{\partial}{\partial z},$$

and we can write

$$F(q) = Aq + a, \quad A := \begin{pmatrix} -\Gamma & 0 \\ 0 & -\gamma \end{pmatrix}, \quad a := \begin{pmatrix} 0 \\ \gamma \end{pmatrix}, \quad G(q) = Bq, \quad B := \begin{pmatrix} 0 & -1 \\ 1 & 0 \end{pmatrix}.$$

The system can be lifted on the semi-direct product $\mathrm{GL}(2, \mathbb{R}) \times_s \mathbb{R}^2$ acting on the q-space by the action $(A, a) \cdot q := Aq + a$, and where the Lie bracket rule is: $[(A, a), (B, b)] := -([A, B], Ab - Ba)$, with $[A, B] := AB - BA$ the commutator. One writes

$$A = \mu\, I_2 + \begin{pmatrix} \alpha & 0 \\ 0 & -\alpha \end{pmatrix},$$

with $\mu := -\frac{\Gamma+\gamma}{2}$, which is zero if and only if $\gamma = -\Gamma$ and $\alpha := \frac{\delta}{2}$, where $\delta := \gamma - \Gamma$. The case $\delta = 0$ is the case of *water species*. Otherwise, we have:

Lemma 3.1. *If $\delta \neq 0$, the Lie algebra generated by (A, a), $(B, 0)$ is $\mathrm{gl}(2, \mathbb{R}) \oplus \mathbb{R}^2$.*

This provides a *rough* classification of the problems between the simple water case and the general case. Moreover, all the Lie brackets can be easily computed. They are listed next, up to length 4.
Length 2.

$$[F, G](q) = (\delta\, z - \gamma)\frac{\partial}{\partial y} + \delta\, y\frac{\partial}{\partial z}.$$

Length 3.

$$[F, [F, G]](q) = \big(\gamma\,(\gamma - 2\Gamma) - \delta^2\, z\big)\,\frac{\partial}{\partial y} + \delta^2\, y\frac{\partial}{\partial z},$$
$$[G, [F, G]](q) = 2\,\delta\, y\frac{\partial}{\partial y} + (\gamma - 2\,\delta\, z)\frac{\partial}{\partial z}.$$

Length 4.

$$\begin{aligned}[F, [F, [F, G]]](q) &= (\gamma\,\Gamma\,(\gamma - 2\Gamma) - \gamma\,\delta^2 + \delta^3\, z)\frac{\partial}{\partial y} + \delta^3 y\frac{\partial}{\partial z}\\ &= \gamma\,\Gamma\,(\gamma - 2\Gamma)\frac{\partial}{\partial y} + \delta^2\,[F, G](q),\\ [G, [F, [F, G]]](q) &= [F, [G, [F, G]]](q) = -\gamma\,(\gamma - 2\Gamma)\frac{\partial}{\partial z},\\ [G, [G, [F, G]]](q) &= (\gamma - 4\,\delta\, z)\frac{\partial}{\partial y} - 4\,\delta\, y\frac{\partial}{\partial z} = -3\,\gamma\frac{\partial}{\partial y} - 4\,[F, G](q).\end{aligned}$$

3.2. **Frame curves, collinearity and singular loci.** The *collinearity locus* $\mathscr{C}$ is defined as the set where F and G are linearly dependent and the *singular set* $\mathscr{S}$ is where F and $[F, G]$ are collinear. Computing, one has:

Lemma 3.2. *The collinearity set $\mathscr{C}$ is given by $\gamma z(1 - z) - \Gamma y^2 = 0$, thus O and N belong to $\mathscr{C}$. Under the assumption $0 < \gamma \leq 2\Gamma$, $\mathscr{C}$ is an ellipse contained in the Bloch ball. Besides, for each point q of $\mathscr{C}$, except O, there exists u such that q is an equilibrium point of the dynamics $F + u\, G$.*

The dynamics reads $F(q) + u\, G(q) = Mq + a$, $M := A + u\, B$, so for the maximal amplitude $u = +1$, the corresponding equilibrium point is

$$O_1 := -M^{-1}a = \frac{\gamma}{u^2 + \gamma\,\Gamma}\begin{pmatrix}-u\\ \Gamma\end{pmatrix} = \frac{\gamma}{1 + \gamma\,\Gamma}\begin{pmatrix}-1\\ \Gamma\end{pmatrix} \in \mathscr{C}$$

and it is contained in the sector $y < 0$. We define in the same way O_{-1} for $u = -1$.

Lemma 3.3. *The singular trajectories are located on $\mathscr{S}$ which is given by $y(\gamma - 2\delta z) = 0$. Hence, it is the union of the z-axis of revolution $y = 0$ and the horizontal line $z = \gamma/(2\delta)$, providing $\delta \neq 0$. Under the assumption $0 < \gamma \leq 2\Gamma$, $\mathscr{S}$ intersects the Bloch ball if and only if $3\gamma \leq 2\Gamma$. In this case, $z_s := \gamma/(2\delta) \in [-1\,, 0)$.*

The singular control is given by solving

$$D'(q) + u\, D(q) = 0,$$

with $D := \det(G,[G,[F,G]])$ and $D' := \det(G,[F,[F,G]])$. For $y=0$, $D(q) = -z(\gamma-2\delta z)$ and $D'=0$. Hence, the singular control is zero and the singular trajectories are solution of $\dot y = -\Gamma y = 0$, $\dot z = \gamma(1-z)$. The North Pole is an equilibrium which is a stable node for $0<\gamma\leq 2\Gamma$. Along the horizontal singular line, *i.e.* for $z=\gamma/(2\delta)$, one has $D(q)=-2\delta y^2$, $D'(q)=\gamma y(2\Gamma-\gamma)$ and the singular control denoted u_s is given by $u_s(q) := \gamma(2\Gamma-\gamma)/(2\delta y)$. Hence, along the singular horizontal direction, the singular flow is: $\dot y = -\Gamma y - \gamma^2(2\Gamma-\gamma)/(4\delta^2 y)$, $\dot z = 0$, and one has $u_s \to \pm\infty$ when $y\to 0^{\mp}$.

Main assumptions. Under the physical assumptions $0<\gamma\leq 2\Gamma$, the Bloch ball is invariant for the dynamics. Besides, under the physical assumption and $|\delta|<2$, any positive bang arc solution of $\dot q = F(q)+G(q) = Mq+a$ spirals around O_1 and converges to it (O_1 is a stable spiral), since in this case M has two complex conjugate eigenvalues with negative real part. Likewise, negative bang arcs spirals around O_{-1}.

Lemma 3.4. *If $\gamma>0$ and $|\delta|<2$, then the solution of $\dot q = F(q)+G(q)$, $q(0)=q_0$ is given by:*

$$q(t) = \exp((\alpha-\gamma)t)\begin{pmatrix} \frac{\alpha}{\beta}\sin(\beta t)+\cos(\beta t) & -\frac{1}{\beta}\sin(\beta t) \\ \frac{1}{\beta}\sin(\beta t) & -\frac{\alpha}{\beta}\sin(\beta t)+\cos(\beta t)\end{pmatrix}(q_0-O_1)+O_1,$$

where $\alpha=\delta/2$ and $\beta := \sqrt{1-\alpha^2}$. The solution is quasi-periodic of period $T := \frac{2\pi}{\beta}$.

Lemma 3.5. *Let $(y(\cdot),z(\cdot))$, with associated control $u(\cdot)$, be a trajectory solution of (2). Then, $(-y(\cdot),z(\cdot))$ with control $-u(\cdot)$ is also solution of (2).*

This discrete symmetry allows us to consider only trajectories in the domain $y\leq 0$ of the Bloch ball.

Notation. We denote by S_1 the intersection of the positive bang arc σ_+ issued from the North Pole with the horizontal singular line $z=z_s=\gamma/(2\delta)$, and by S_1' the intersection with the vertical singular line $y=0$. S_1 and S_1' may not exist for specific values of (γ,Γ). We denote by S_3 the point on the horizontal singular line such that σ_+ is tangent to this line at this point, *i.e.* S_3 is a saturation point for the singular control u_s ($u_s(S_3)=1$), and by S_3' the intersection of the bang arc σ_+ issued from S_3 with the axis $y=0$. If $0<\gamma\leq 2\Gamma$ is satisfied, then S_3 is in the domain $y<0$ if $\delta<0$. We define in the same way S_{-3} for $u=-1$. See the left sub-graph of Fig. 1 to visualize on an example: the singular and collinearity sets, the points S_1, S_1', S_3, S_3'...

3.3. Switching function, the concept of bridge and the Θ function.

3.3.1. *Switching function.* Let $z(t)$, $t\in[0\,,T]$, be an extremal curve. The *switching function* is defined as $\Phi(t) := p(t)\cdot G(q(t))$. A time t is called an *ordinary switching time* if $\Phi(t)=0$ and $\dot\Phi(t)\neq 0$, *i.e.* $p(t)\cdot G(q(t))=0$ and $p(t)\cdot[F,G](q(t))\neq 0$. In the 2D-case, outside the collinearity set, one can write $[F,G](q)=\alpha(q)\,F(q)+\beta(q)\,G(q)$, with

$$\alpha(q) = \frac{\det(G(q),[F,G](q))}{\det(G(q),F(q))}.$$

At an ordinary switching time t, one has $\mathrm{sign}(\dot\Phi(t)) = \mathrm{sign}(\alpha(q(t)))$, with the convention of the maximum principle, *i.e.* $H_F\geq 0$. If $\alpha(q(t))>0$, then we switch

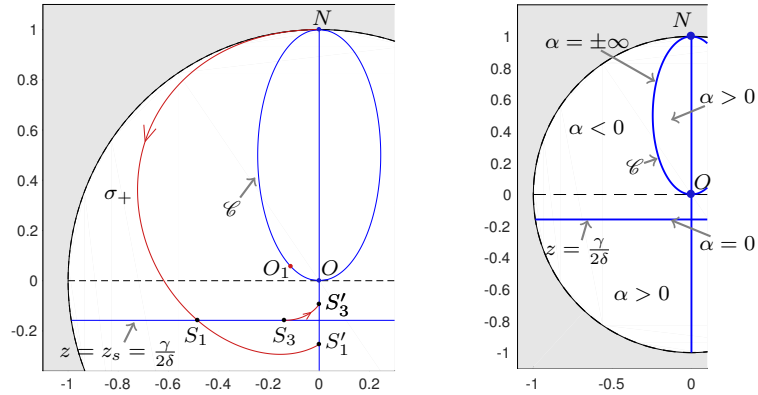

FIGURE 1. In this example, $(\gamma, \Gamma) = (0.12, 0.5)$. (Left) Collinearity set, singular set and visualization of N, O, O_1, S_1, S_1', S_3 and S_3'. (Right) Sign of $\alpha(q)$ in the domain $y \leq 0$. The sign in the domain $y \geq 0$ is given by symmetry.

from an arc σ_- to an arc σ_+ and the converse if $\alpha(q(t)) < 0$. The right sub-graph of Fig. 1 gives the sign of α inside the Bloch ball for $(\gamma, \Gamma) = (0.12, 0.5)$.

3.3.2. *The concept of Bridge.* An arc σ_+ or σ_- corresponding to $u = +1$ or $u = -1$, is called a *bridge* on $[0\,, t]$ if the extremities correspond to non ordinary switching points, *i.e.* $\Phi(0) = \dot{\Phi}(0) = \Phi(t) = \dot{\Phi}(t) = 0$.

Remark 1. This concept is important and leads to a generalization in higher dimension, which plays an important role in the time minimal saturation of a pair of spins, but also in the contrast problem.

Notation. If a bridge σ_+, in the domain $y \leq 0$, connecting the horizontal and vertical singular lines exists, then we denote by S_2 the extremity on $z = \gamma/(2\delta)$, and S_2' the other extremity on $y = 0$. We observe two cases when S_2 exists which are crucial for the analysis of the time minimal saturation problem of a single spin, see Fig. 2.

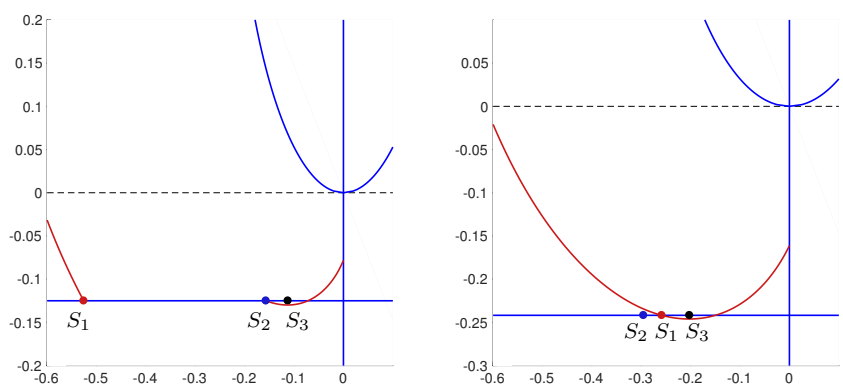

FIGURE 2. The points S_1, S_2 and S_3 with different orders. Left sub-graph: $(\gamma, \Gamma) = (0.1, 0.5)$ and right: $(\gamma, \Gamma) = (0.163, 0.5)$.

3.3.3. *Analysis of two consecutive switching times.* In the 2D-case, in order to analyze switchings, one proceeds as follows. Assume 0 and t be two consecutive switching times on an arc σ_+ or σ_-. Let $z(\cdot) := (q(\cdot), p(\cdot))$ denote the associated extremal. We have:

$$p(0) \cdot G(q(0)) = p(t) \cdot G(q(t)) = 0.$$

We denote by $v(\cdot)$ the solution on $[0\,,t]$ of the variational equation

$$\dot{v}(s) = \left(\frac{\partial F}{\partial q}(q(s)) + u\,\frac{\partial G}{\partial q}(q(s))\right) v(s), \quad v(t) = G(q(t)), \quad u = \pm 1.$$

This equation is integrated backwards from time t to 0. We have by definition

$$v(0) = e^{-t\,\mathrm{ad}(F+u\,G)}(G(q(t))), \quad u = \pm 1,$$

and in the analytic case, the ad-formula gives:

$$v(0) = \sum_{n\geq 0} \frac{(-t)^n}{n!}\,\mathrm{ad}^n(F + u\,G) \cdot G(q(t)).$$

The computation can be made explicit on a Lie group since determining $\exp(t\,\mathrm{ad}(F+u\,G))$ amounts to compute a Jordan form of the linear operator $\mathrm{ad}(F+u\,G)$ defined by the Lie brackets.

By construction, $p(\cdot) \cdot v(\cdot)$ is constant and equal to zero. At time 0, one has $p(0) \cdot v(0) = p(0) \cdot G(q(0)) = 0$. Hence, $p(0)$ is orthogonal to $v(0)$ and to $G(q(0))$. Therefore, $v(0)$ and $G(q(0))$ are collinear ($p(\cdot)$ does not vanish, according to proposition 1). We introduce naturally the $\Theta(t)$ function [14] which gives the angle between $G(q(0))$ and $v(0)$ measured counterclockwise. One deduces that switchings occur at times 0 and t if

$$\Theta(t) = 0 \mod \pi$$

and it can be tested using $\det(G(q(0)), v(0)) = 0$. This test may be used by contraposition in order to eliminate the possibility that bang-bang trajectories with at least two switching times (or more) are optimal.

3.4. **Optimality status.** A first step in the optimality analysis is to discriminate between small time minimizing or maximizing singular trajectories using the high-order maximum principle and Theorem 2.2. In dimension 2, we introduce $D'' := \det(G, F)$ and $D'' = 0$ is the collinearity set $\mathscr{C}$. Singular lines are hyperbolic if $D\,D'' > 0$ and elliptic if $D\,D'' < 0$. Using these conditions, if $0 < \gamma$ and $\delta < 0$, then the horizontal singular line $z = z_s$ is hyperbolic, except at $y = 0$. For the interesting case when the horizontal singular line cuts the Bloch ball, *i.e.* when $0 < 3\gamma \leq 2\Gamma$, the singular horizontal line is parabolic on $(S_3\,, S_{-3}) = \{(1-\lambda)S_3 + \lambda S_{-3} \mid \lambda \in (0\,,1)\}$ when $y \neq 0$. On the other hand, assuming $0 < \gamma \leq 2\Gamma$ and considering only the interesting part inside the Bloch ball, then we have the following: if $\delta < 0$, then the vertical line is hyperbolic for $z_s < z < 1$ and elliptic for $-1 \leq z < z_s$. If $\delta > 0$, then it is hyperbolic for $-1 \leq z < 1$.

Theorem 2.2 combined with the generalized Legendre-Clebsch condition gives information about the local optimality of the singular extremals. In the 2D-case, global optimality can be analyzed using the clock form $\omega = p \cdot \mathrm{d}q$ with $p \cdot G = 0$ and $p \cdot F = 1$. The clock form may be used to compare two trajectories with the same extremities whenever they do not cross the collinearity set. In the time minimal saturation problem of a single spin, the collinearity set plays a crucial role and we

must use the Θ function defined in section 3.3 to eliminate the possibility to have two consecutive ordinary switching times.

To complete the study, we have to analyze the behavior of optimal trajectories in the neighborhood of some particular points, named *Frame Points* [14] corresponding to isolated singularities: intersection of the collinearity locus with singular locus or singular loci. In the time minimal saturation problem, there exists two phenomena to analyze. The horizontal singular line being admissible up to a saturation point S_3, there is a birth of a switching locus connecting the horizontal and vertical singular lines. This is related to the concept of bridge and this phenomenon is referred as the SiSi singularity [10]. The time minimal synthesis, with initial point N, is represented on Figs. 6, 7 and 8. The interaction between the collinearity and singular sets near the North Pole is the second phenomenon to analyze and is referred as the SiCo singularity [10]. Near the North Pole, only bang-bang trajectories with at most one switching are optimal (see the top part of Fig. 6).

According to the sections 3.5, 3.6, 3.7 and 3.8 and according to the Figs. 6, 7 and 8, we have the following results.

Theorem 3.6. *Let us denote by σ_+^N the positive bang arc starting from the North Pole with S_1, S_1' respectively the intersection points (they may not exist) with the horizontal, vertical singular line. Let us denote by σ_+^b the bridge with S_2 and S_2' as extremities, by σ_s^h, σ_s^v respectively a horizontal, vertical singular arc. Let S_3 denote the saturation point on the horizontal singular line and S_3' the intersection of the bang arc starting from S_3 with the axis $y = 0$.*

For parameters (Γ, γ) satisfying the physical constraints $0 < \gamma \leq 2\Gamma$, and such that the points S_1' and S_3' are below the origin O, then the minimal time trajectory to steer the spin from N to O is $NS_1S_2S_2'O$, i.e. it is of the form $\sigma_+^N\sigma_s^h\sigma_+^b\sigma_s^v$ (no empty arcs), if σ_+^N intersects the horizontal singular line strictly before S_2, that is $S_1 < S_2$. Otherwise, the optimal trajectory is $NS_1'O$, i.e. of the form $\sigma_+^N\sigma_s^v$.

3.5. **Parameters and practical cases.** The optimal syntheses depend on the parameters (γ, Γ). We define in this section the domain of interest of the parameters and partition it in four main sub-domains which are denoted A_1, A_2, B and C. This partitioning may be visualized on Fig. 3.

We have already seen that we assume $0 < \gamma \leq 2\Gamma$ and $|\delta| < 2$, with $\delta = \gamma - \Gamma$. Additionally, we require that the origin O is accessible from the North Pole N, that is we impose that S_1' is below O. The parameters such that $S_1' = O$ are given by the following result.

Lemma 3.7. *For $\gamma > 0$, we have:*

$$S_1' = O \Longleftrightarrow \exp\left((t_0\,\beta + \pi)\,\frac{\alpha - \gamma}{\beta}\right) - \gamma = 0,$$

with

$$t_0 := \begin{cases} \frac{1}{\beta}\arctan\left(-\frac{\beta}{\alpha}\right) & \text{if} \quad \delta < 0, \\ \frac{\pi}{2} & \text{if} \quad \delta = 0, \\ \frac{1}{\beta}\left(\arctan\left(-\frac{\beta}{\alpha}\right) + \pi\right) & \text{if} \quad \delta > 0. \end{cases}$$

Besides, to simplify the presentation, we restrict the analysis to the case where S_3' is below O. This implies that the origin may be reached from the horizontal singular locus going through the bridge. We have the following relation on the parameters to impose $S_3' = O$:

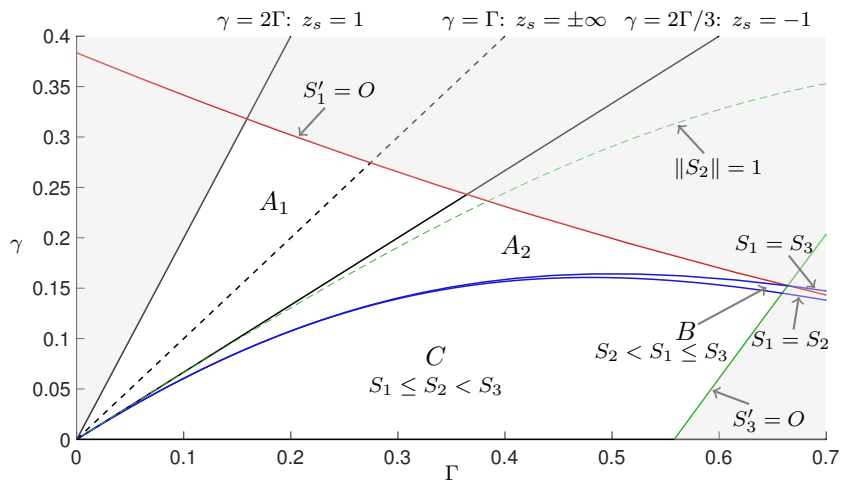

FIGURE 3. The domain of interest of the parameters in white with the sub-domains A_1, A_2, B and C.

Lemma 3.8.

$$S_3' = O \Longleftrightarrow (2\Gamma^2 - \gamma\Gamma + 1)\exp\left((\alpha - \gamma)t_0\right) - 2|\delta| = 0.$$

One can notice according to Fig. 3 that if $0 < \gamma \leq 2\Gamma$ is satisfied and if the points S_1' and S_3' are below the origin O, then $|\delta| < 2$ automatically holds. The remark 2 justifies why we restrict the analysis to these values of parameters.

Let us explain now how we partition this domain. We denote by A_1 the sub-domain such that $2\Gamma/3 \leq \gamma \leq 2\Gamma$ and S_1' is below O. In this case, S_3' is necessarily below O, the horizontal singular line (at $z = z_s = \gamma/(2\delta)$) does not cut the interior of the Bloch ball and the optimal synthesis is simple, see section 3.8. Now, when the horizontal singular line cuts the interior of the Bloch ball, that is for $0 < \gamma < 2\Gamma/3$, this part of the singular locus does not play any role if the bang arc starting from the North Pole does not intersect it, that is if S_1 does not exist. The limit case is when $S_1 = S_3$, where S_3 is the saturation point on the horizontal singular line.

Lemma 3.9.

$$S_1 = S_3 \Longleftrightarrow (2\Gamma^2 - \gamma\Gamma + 1)\frac{\gamma}{2\delta} + \exp\left((\alpha - \gamma)\frac{\pi}{\beta}\right) = 0.$$

We denote by A_2 this sub-domain of parameters and we have the same optimal syntheses in A_1 and A_2, see again section 3.8. The remaining part, when S_1 exists, may be split in two. Either, S_1 is before S_2 (S_2 is one of the extremities of the bridge) or after, see Fig. 2. We denote by B the sub-domain where $S_1 > S_2$ (*i.e.* S_2 strictly before S_1) and C where $S_1 \leq S_2$. One can visualize the sub-domains A_1, A_2, B and C on the Fig. 3.

Remark 2. Each species to study is characterized by its relaxation times T_1 and T_2, see Table 1. However, the main parameter is the ratio T_2/T_1. According to Fig. 4, one can see that for any couple (T_1, T_2) such that $0 < T_2 < 2T_1/3$, then there exists $\omega_{\max} > 0$ such that the associated parameters (γ, Γ), see eq. (1), belongs to C. Hence, for any couple (T_1, T_2) satisfying the physical constraint $0 < T_2 \leq 2T_1$, there exists $\omega_{\max} > 0$ such that the associated parameters (γ, Γ) belongs either to A_1 or C.

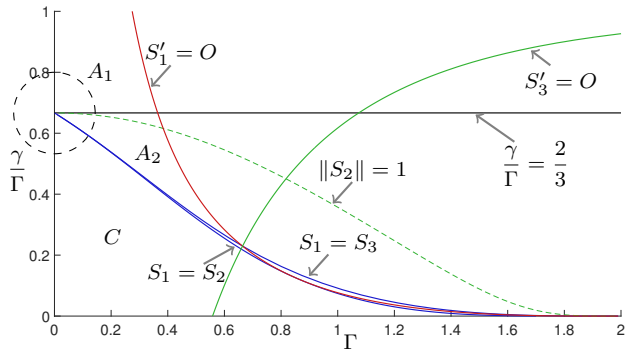

FIGURE 4. The sub-domains in $(\Gamma, \gamma/\Gamma)$ coordinates. One can notice that when Γ tends to 0, then the slopes of the curves $S_1 = S_2$ and $S_1 = S_3$, in (Γ, γ) coordinates, are equal to $2/3$.

In Fig. 5 is represented the slope $T_2/T_1 = \gamma/\Gamma$ with the particular case when $\omega_{\max} = 2\pi \times 32.3$ Hz. The fat case is the only one which crosses the sub-domains A_2, B and C. Note that in the experiments, $\omega_{\max}$ may be chosen up to 15 000 Hz but we consider here the same value as in [10]. With this value of $\omega_{\max}$, the water case belongs to the domain A_1 while all the others cases are contained in C.

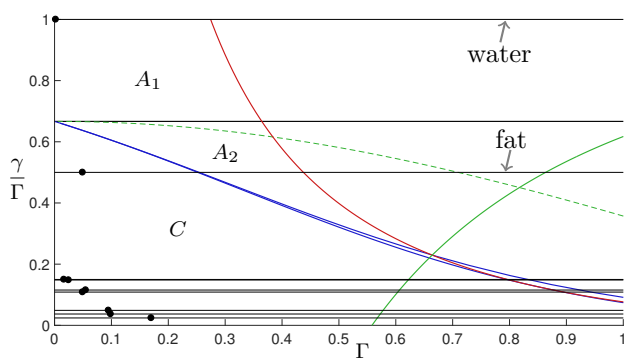

FIGURE 5. The slopes $T_2/T_1 = \gamma/\Gamma$ for the species from Table 1 with the particular case when $\omega_{\max} = 2\pi \times 32.3$ Hz. This case is represented by a bullet while the slope is represented by a line.

3.6. **The optimal synthesis in the sub-domain C.** For the optimal synthesis in the sub-domain C, we have the following: the parameters satisfy $0 < 3\gamma < 2\Gamma$, the point S_3' is below the origin O and there exist S_1 and S_2 such that $S_1 \leq S_2 < S_3$, *i.e.* we are in the situation of the left sub-graph of Fig. 2. In this case, the horizontal singular line cuts the Bloch ball in the domain $-1 < z < 0$ and the global synthesis is similar to the one presented in [10]. It is obtained gluing together the SiSi and SiCo singularities and it is represented on the Fig. 6.

Remark 3. In [10], to obtain this optimal synthesis, it is assumed that $\omega_{\max}$ is large enough. Remark 2 explains why this assumption is correct. However, this assumption is replaced here by geometric relations on the points S_1, S_2 and S_3'.

The switching locus is formed by the positive bang arc starting from the North Pole (denoted σ_+^N) and reaching the horizontal singular arc at S_1 (it is denoted Σ_1

in the figure), by the horizontal singular segment Σ_2 between the points S_1 and S_3, the switching locus Σ_3 due to the saturation phenomenon and by the part of the vertical singular direction between S_2' and O (the Σ_4 segment), S_2' being the extremity of the bridge on $y = 0$. The bang arc with $u = -1$ starting from S_1 splits the domain in two sub-domains, one with a bang-bang policy and the other containing a non trivial singular arc.

We have, as a corollary, that in this case, the optimal strategy to steer the system from the North Pole to the origin in minimum time is of the form $\sigma_+^N \sigma_s^h \sigma_+^b \sigma_s^v$, where σ_s^h and σ_s^v denote respectively horizontal and vertical singular arcs, and where σ_+^b is the bridge.

Remark 4. Note that the switching locus has a complex structure, but due to the symmetry, all the cut points, i.e. the first points where the extremal trajectories cease to be optimal, are on the vertical z-axis where two symmetric solutions starting respectively on the left and right part of the Bloch ball intersect at the same time.

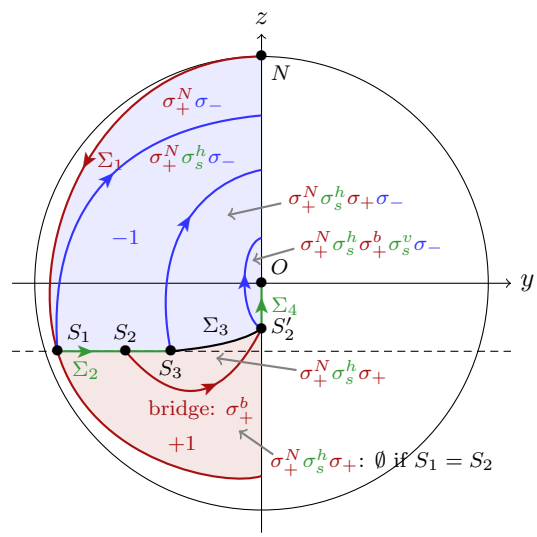

FIGURE 6. Schematic time minimal synthesis to steer a single spin system from the North Pole N to any point of the Bloch ball in the reachable set, for parameters $(\Gamma, \gamma) \in C$. An arbitrary zoom has been used to construct the figure. The set of Σ_i forms the switching surface Σ dividing the $+1$ and -1 areas respectively in red and blue. The minimal time trajectory to steer the spin from N to O is $NS_1S_2S_2'O$, *i.e.* it is of the form $\sigma_+^N \sigma_s^h \sigma_+^b \sigma_s^v$ with horizontal σ_s^h and vertical σ_s^v singular arcs. The spin leaves the horizontal singular arc before the point S_3 (where the control saturates the constraint) producing a bridge σ_+^b to reach the vertical singular line.

3.7. **The optimal synthesis in the sub-domains B.** For the optimal synthesis in the sub-domain B, we have the following: the parameters satisfy $0 < 3\gamma < 2\Gamma$, the point S_3' is below the origin O and there exist S_1 and S_2 such that $S_2 < S_1 \leq S_3$, *i.e.* we are in the situation of the right sub-graph of Fig. 2. In this case, the horizontal singular line cuts the Bloch ball in the domain $-1 < z < 0$ and still plays a role.

The switching locus is formed by the positive bang arc starting from the North Pole (denoted σ_+^N) and reaching the horizontal singular arc at S_1 (denoted Σ_1), by the horizontal singular segment Σ_2 between the points S_1 and S_3, by the switching locus Σ_3 due to the saturation phenomenon from S_3 to the intersection with σ_+^N (denoted S_1''), by the part of σ_+^N between S_1'' and S_1' (denoted Σ_5) and by the part of the vertical singular direction between S_1' and O (the Σ_4 segment), S_1' being the extremity of σ_+^N on $y = 0$.

We have, as a corollary, that in this case, the optimal strategy to steer the system from the North Pole to the origin in minimum time is of the form $\sigma_+^N \sigma_s^v$.

Remark 5. The switching locus is on the vertical z-axis due to the symmetry.

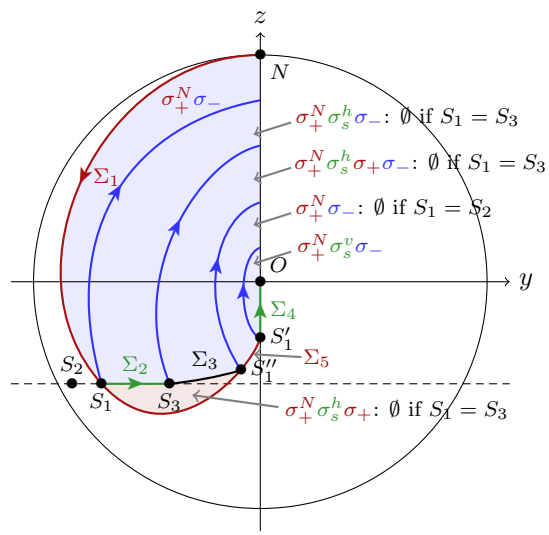

FIGURE 7. Schematic time minimal synthesis to steer a single spin system from the North Pole N to any point of the Bloch ball in the reachable set, for parameters $(\Gamma, \gamma) \in B$. An arbitrary zoom has been used to construct the figure. The set of Σ_i forms the switching surface Σ dividing the $+1$ and -1 areas respectively in red and blue. The minimal time trajectory to steer the spin from N to O is $NS_1'O$, *i.e.* it is of the form $\sigma_+^N \sigma_s^v$.

3.8. **The optimal synthesis in the sub-domains A_1 and A_2.** For the optimal synthesis in the sub-domains A_1 and A_2, we have the following: the parameters satisfy $0 < \gamma \leq 2\Gamma$, the point S_1' is below the origin O and σ_+^N does not intersect the horizontal singular line $z = z_s = \gamma/(2\delta)$, that is S_1 does not exist. In this case, the horizontal singular line does not play any role.

The switching locus is formed by the positive bang arc starting from the North Pole (denoted σ_+^N) and reaching the vertical singular arc at S_1' (denoted Σ_1) and by the part of the vertical singular direction between S_1' and O (the Σ_4 segment).

We have, as a corollary, that in this case, the optimal strategy to steer the system from the North Pole to the origin in minimum time is of the form $\sigma_+^N \sigma_s^v$ as in the sub-domain B.

Remark 6. The switching locus is on the vertical z-axis due to the symmetry.

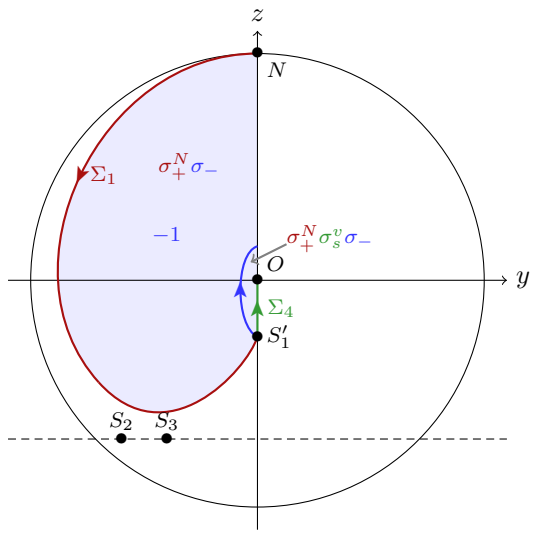

FIGURE 8. Schematic time minimal synthesis to steer a single spin system from the North Pole N to any point of the Bloch ball in the reachable set, for parameters $(\Gamma, \gamma) \in A_2$. For $(\Gamma, \gamma) \in A_1$, the synthesis is the same but there is no horizontal singular line inside the Bloch ball. An arbitrary zoom has been used to construct the figure. The minimal time trajectory to steer the spin from N to O is $NS_1'O$, *i.e.* it is of the form $\sigma_+^N\sigma_s^v$.

4. **Bi-saturation: the model and prior theoretical results.**

4.1. **The model.** Let us consider a couple of spins with the same characteristics, *i.e.* the same relaxation times T_1 and T_2, but for which for each, the control field has different intensities, because of inhomogeneities. The system we consider is the following:

$$\dot{q}_1(t) = F(q_1(t)) + u(t)\, G(q_1(t)),$$
$$\dot{q}_2(t) = F(q_2(t)) + u(t)\,(1-\varepsilon)\, G(q_2(t)),$$

where $q_i := (y_i, z_i)$, $i = 1, 2$, denote the coordinates of each system and where the vector fields F and G are given by eq. (2), see sections 2.1 and 3.1. The term $(1-\varepsilon)$, $\varepsilon > 0$ small, is the rescaling factor of the control maximal amplitude. We define the *time minimal saturation problem of a pair of spin-1/2 particles* (or bi-saturation problem) as the following affine control problem with Mayer cost:

$$(\mathrm{P_{BS}}) \quad \begin{cases} J(u(\cdot), t_f) := t_f \longrightarrow \min \\ \dot{q}(t) = F(q(t)) + u(t)\, G(q(t)), \quad |u(t)| \leq 1, \quad t \in [0\,, t_f], \quad q(0) = q_0, \\ q(t_f) = q_f, \end{cases}$$

where $q := (q_1, q_2) = (y_1, z_1, y_2, z_2)$, $q_0 := (0, 1, 0, 1)$, $q_f := (0, 0, 0, 0)$, and where we use the notation

$$F(q) := F(q_1)\frac{\partial}{\partial q_1} + F(q_2)\frac{\partial}{\partial q_2}, \quad G(q) := G(q_1)\frac{\partial}{\partial q_1} + (1-\varepsilon)\, G(q_2)\frac{\partial}{\partial q_2}.$$

Note that we use the same notations (no confusion is possible) for the vector fields F and G in the mono and bi-saturation cases. We have the following Lie brackets up to order 3:

$$[F,G](q) = [F,G](q_1)\frac{\partial}{\partial q_1} + (1-\varepsilon)\,[F,G](q_2)\frac{\partial}{\partial q_2},$$

$$[F,[F,G]](q) = [F,[F,G]](q_1)\frac{\partial}{\partial q_1} + (1-\varepsilon)\,[F,[F,G]](q_2)\frac{\partial}{\partial q_2},$$

$$[G,[F,G]](q) = [G,[F,G]](q_1)\frac{\partial}{\partial q_1} + (1-\varepsilon)^2\,[G,[F,G]](q_2)\frac{\partial}{\partial q_2}.$$

The limit case when $\varepsilon = 0$ brings us back to the time minimal saturation of a single spin (or mono-saturation problem). It is obvious that the bi-saturation problem (with $\varepsilon > 0$) is much more complex than the mono-saturation problem. The bi-saturation problem is in dimension 4 and has a complex singular flow which of course do not reduce to two lines in the state space. To any point of the state space, we have an infinity of singular extremals passing through this point. For these reasons, we do not aim to determine any optimal synthesis. The first important step is to analyze the singular extremals in relation with the concept of bridge. See section 3.3.2 for the concept of bridge and section 5 for the analysis of the singular extremals with algebraic techniques. This analysis gives geometric insights of the singular flow.

On the other hand, one can use numerical methods to obtain numerical candidates as minimizers, for instance by the so-called direct collocation methods. In order to validate the global optimality of this candidate, one can use LMI techniques to estimate the gap between the cost of the candidate and the optimal cost. This LMI validation, presented in section 6, gives good confidence rate on global optimality. This step is important due to the existence of many local optima in the bi-saturation problem. Note that we compute the gap also in the mono-saturation case where we have the optimal solution to evaluate the part in the gap which is due to numerical errors.

Finally, in section 7 we study the influence of the parameters on BC-extremals, that is extremals satisfying the Pontryagin Maximum Principle. One important point would be to be sure to analyze the optimal solutions but proving global optimality is a very difficult task and we analyze only the best BC-extremals we found. This means that we have to compare different BC-extremals since again, in the bi-saturation problem, as in the contrast problem [8], there exist many locally optimal solutions. The bi-saturation problem has three parameters: γ, Γ and ε. In section 7, we fix ε and $\gamma^2+\Gamma^2$ and present three different solutions which emphasize the complex structure of the singular flow, analyzed in section 5.

4.2. **Some prior theoretical results.** We present some prior theoretical results in relation with Fig. 14 from section 7. They are based on Lie brackets computations.

Lemma 4.1. $\mathrm{span}\{\mathrm{ad}^k F\cdot G;\ k\geq 0\} = \mathrm{span}\{\mathrm{ad}^k F\cdot G;\ k=0,1,2,3\}$.

Proposition 4. *For all q in the Bloch ball, for all pair of parameters (Γ,γ), we have* $\det(G(q),[F,G](q),[F,[F,G]](q),[F,[F,[F,G]]](q)) = 0$ *and every solution of $F(q)$ is a (smooth) singular trajectory.*

Lemma 4.2. *In the water case $\gamma=\Gamma$,* $\mathrm{ad}^2 F\cdot G$ *is constant and collinear to $[F,G]$.*

Proposition 5. *In the water case $\gamma = \Gamma$, the only singular trajectories, projections of singular extremals of minimal order, are the (smooth) solutions of $F(q)$.*

4.3. **A geometric remark.** The Lie algebraic computation led to an important geometric property. For a single spin the optimal analysis boils down to two cases. In the first case, the time minimal solution used the horizontal singular line and its singularity to generate a bridge. In the second case, the time minimal solution corresponds to the standard inversion solution using the vertical line only, avoiding singularities. For a pair of spins, this phenomenon persists. But the singularity analysis is much more intricate and led to the computations of section 5.

5. **Bi-saturation: algebraic techniques and singularity analysis.** The `Maple` symbolic software is used to perform algebraic computations related to singularity analysis of the extremal trajectories, in particular in relation with the determination of bridges. The computations boil down to the computation of Gröbner bases and one needs the following concepts and techniques of this area which are used in the proofs.

5.1. **Operation on polynomial ideals.** This section will involve different transformations of polynomial equations in order to classify their roots. We briefly recall the definitions of some of those operations.

More precisely, let n be a positive integer, and consider polynomials in $A := \mathbb{C}[X_1, \dots, X_n]$. Given a system of equations $\mathcal{F}$, consider the set $V(\mathcal{F}) \subset \mathbb{C}^n$ of zeroes of $\mathcal{F}$. Such sets are called *algebraic sets*.

The main object of study is the ideal $I = \langle \mathcal{F} \rangle$. The common zeroes of the polynomials in I are exactly the zeroes of $\mathcal{F}$. In other words, $V(\mathcal{F}) = V(I)$.

Given an ideal I and a polynomial f, *saturating* I by f means computing a set of generators of the ideal

$$(I : f^\infty) := \{g \in A, \exists\, m \in \mathbb{N}, gf^m \in I\}.$$

The zeroes of $(I : F^\infty)$ form the smallest algebraic set containing $V(I) \setminus V(\{f\}))$. Computing generators of $(I : f^\infty)$ can be done with a Gröbner basis computation.

Given an ideal I, its *radical* is the set

$$\sqrt{I} := \{f \in A, \exists\, m \in \mathbb{N}, f^m \in I\}.$$

This ideal has the property that

$$V(\sqrt{I}) = V(I)$$

and $\sqrt{I}$ is the largest ideal with this property: any polynomial vanishing on $V(I)$ lies in $\sqrt{I}$.

Computing the radical of I can be done, but it is a complicated process. On the other hand, an easier computation is that of an ideal J such that $I \subseteq J \subseteq \sqrt{I} = \sqrt{J}$. Indeed, define the *square-free form* of a polynomial as follows: given f be a polynomial in A with decomposition as a product of irreducibles $f = p_1^{e_1} \cdots p_r^{e_r}$, its square-free form is

$$\mathsf{sqfr}(f) = p_1 \cdots p_r.$$

Then, given a set of generators $f_1, \dots, f_k$ of I, one can take the ideal

$$J = \langle \mathsf{sqfr}(f_1), \dots, \mathsf{sqfr}(f_1) \rangle$$

5.2. **Frame curves.** We present the frame curves associated to the saturation of a pair of spins.

5.2.1. *Collinearity locus.* $\mathcal{C}$ is defined as the set where F and G are linearly dependent. Outside zero, it is defined by: $\exists\lambda$ such that $F = \lambda G$, that is:

$$\Gamma y_1 = \lambda z_1, \quad \gamma(1-z_1) = \lambda y_1, \quad \Gamma y_2 = \lambda z_2\,(1-\varepsilon), \quad \gamma(1-z_2) = \lambda y_2\,(1-\varepsilon),$$

The projections on q_i-spaces are the ovals:

$$\Gamma_i y_i^2 = \gamma\,(1-z_i)z_i, \quad 0 \le z_i \le 1, \quad i = 1,2$$

intersected with one of the sets

$$\Gamma(1-\varepsilon)y_1 z_2 = \Gamma y_2 z_1, \quad (1-\varepsilon)y_2(1-z_1) = y_1(1-z_2).$$

5.2.2. *Singularity locus.* $\mathcal{S}$ is defined as the set where G and $[F,G]$ are linearly dependent. Outside zero, it is defined by: $\exists\lambda$ such that $[F,G] = \lambda\, G$, that is

$$\begin{aligned} \delta\, z_1 - \gamma = -\lambda\, z_1, \quad \delta\, y_1 = \lambda\, y_1, \\ \delta\, z_2 - \gamma = -\lambda\, z_2, \quad \delta\, y_2 = \lambda\, y_2, \end{aligned}$$

Projections on each q_i-spaces will form the two singular lines

$$z_i = \gamma/(2\delta), \quad y_i = 0, \quad i = 1,2.$$

The additional relations define the full locus.

5.3. **Singularity classification: exceptional case $H_F = 0$.**

5.3.1. *Conventions and notations.* For the computations, we use the translation

$$z_1 \leftarrow z_1 + 1, \quad z_2 \leftarrow z_2 + 1, \tag{5}$$

which places the center of the coordinates at the North Pole of the Bloch ball. In this new system of coordinates, the center of the Bloch ball has coordinates $(0,-1,0,-1)$. We have in the exceptional case the constraint

$$p \cdot F = p \cdot G = p \cdot [F,G] = 0,$$

hence p can be eliminated in the relation defining the control

$$p \cdot ([F,[F,G]] + u\,[G,[F,G]]) = 0$$

which is computed as the feedback

$$u_s(q) := -\frac{D'(q)}{D(q)}$$

with

$$\begin{aligned} D &:= \det(F,G,[F,G],[G,[F,G]]) \\ &= \det \begin{bmatrix} -\Gamma y & -z-1 & \delta z - \Gamma & 2\delta y \\ -\gamma z & y & \delta y & -2\delta z + \Gamma - \delta \\ -\Gamma y & (1-\varepsilon)(-z-1) & (1-\varepsilon)(\delta z - \Gamma) & (1-\varepsilon)^2(2\delta y) \\ -\gamma z & (1-\varepsilon)y & (1-\varepsilon)\delta y & (1-\varepsilon)^2(-2\delta z + \Gamma - \delta) \end{bmatrix} \end{aligned} \tag{6}$$

and

$$D' \coloneqq \det(F, G, [F, G], [F, [F, G]])$$
$$= \det \begin{bmatrix} -\Gamma y & -z-1 & \delta z - \Gamma & \gamma(\gamma - 2\Gamma) + \delta^2(z+1) \\ -\gamma z & y & \delta y & \delta^2 y \\ -\Gamma y & (1-\varepsilon)(-z-1) & (1-\varepsilon)(\delta z - \Gamma) & (1-\varepsilon)(\gamma(\gamma - 2\Gamma) + \delta(z+1)) \\ -\gamma z & (1-\varepsilon)y & (1-\varepsilon)\delta y & (1-\varepsilon)\delta^2 y \end{bmatrix}. \quad (7)$$

Using a time reparameterization, this leads to analyze the C^ω-vector field in the q-space

$$X \coloneqq DF - D'G.$$

Moreover, the following polynomials will appear frequently in the remainder of the section:

- $P_{y_1} \coloneqq y_1 - (1-\varepsilon)y_2$,
- $P_{y_2} \coloneqq y_2 - (1-\varepsilon)y_1$,
- $P_{z_1} \coloneqq 2(\Gamma - \gamma)z_1 + 2\Gamma - \gamma$,
- $P_{z_2} \coloneqq 2(\Gamma - \gamma)z_2 + 2\Gamma - \gamma$.

The root of the univariate polynomials P_{z_1} and P_{z_2}, in z_1 and z_2 respectively, is

$$z_S \coloneqq \frac{\gamma - 2\Gamma}{2\Gamma - 2\gamma}. \quad (8)$$

5.3.2. *Singularities of* $\{D = 0\}$.

Proposition 6. *The set of points satisfying* $D = \frac{\partial D}{\partial y_1} = \frac{\partial D}{\partial z_1} = \frac{\partial D}{\partial y_2} = \frac{\partial D}{\partial z_2} = 0$ *is given, generically on authorized values of* γ, Γ, *by*

1. *the point* $y_1 = y_2 = z_1 = z_2 = 0$, *and*
2. *the curve defined by* $P_{y_1} = P_{z_1} = P_{z_2} = 0$, *which is parameterized by* y_2 *as*

$$\begin{cases} y_1 = (1-\varepsilon)y_2 \\ z_1 = z_2 = z_S = \frac{\gamma - 2\Gamma}{2\Gamma - 2\gamma}. \end{cases}$$

If $\gamma = \Gamma$ *(water case), only the former solution exists.*

Proof. The determinant D can be factored as $(1-\varepsilon)\tilde{D}$. The singularities of D and those of $\tilde{D}$ are the same, so for the study, we consider the ideal

$$I \coloneqq \left\langle \tilde{D}, \frac{\partial \tilde{D}}{\partial y_1}, \frac{\partial \tilde{D}}{\partial y_2}, \frac{\partial \tilde{D}}{\partial z_1}, \frac{\partial \tilde{D}}{\partial z_2} \right\rangle.$$

In order to eliminate y_1, y_2 and z_1 from the ideal I, we compute a Gröbner basis $\mathcal{G}$ of I with respect to the elimination ordering $y_1 > y_2 > z_1 \gg z_2 > \varepsilon > \Gamma > \gamma$. This computation yields that

$$I \cap \mathbb{Q}[z_2, \varepsilon, \Gamma, \gamma] = \left\langle \varepsilon^2(\varepsilon - 2)^2(2\,\Gamma - \gamma)(\Gamma - \gamma)z_2^3 P_{z_2}^3 \right\rangle,$$

so singular points necessarily satisfy

$$\begin{cases} z_2 = 0 \\ \text{or} \\ P_{z_2} = 0 \iff z_2 = \frac{\gamma - 2\,\Gamma}{2\,\Gamma - 2\,\gamma}. \end{cases}$$

If $\Gamma = \gamma$ (that is, if the matter is water), the second of these solutions does not exist. If $\gamma = 2\,\Gamma$ (which means that the matter is on the limit of the domain of validity $2\,\Gamma \geq \gamma$), both solutions coincide. In all other cases, there are 2 distinct possible values for z_2, and we consider both cases: we consider the two ideals

$$I_1 \coloneqq \langle \mathsf{sqfr}(\mathcal{G}), z_2 \rangle,$$
$$I_2 \coloneqq \langle \mathsf{sqfr}(\mathcal{G}), P_{z_2} \rangle,$$

where for any polynomial f, $\mathsf{sqfr}(f)$ is the square-free part of f and $\mathsf{sqfr}(\mathcal{G})$ means that we apply sqfr to each element of $\mathcal{G}$.

In order to lift the partial solution $z_2 = 0$, we compute a Gröbner basis $\mathcal{G}_1$ of I_1 with respect to the ordering $y_1 > y_2 \gg z_1 > z_2 > \varepsilon > \Gamma > \gamma$, and we find that this ideal contains $\gamma z_1^2(\varepsilon - 1)^2(2\Gamma - \gamma)$, so $z_1 = 0$. We then compute a Gröbner basis of $\langle \mathsf{sqfr}(\mathcal{G}_1), z_1 \rangle$ with respect to the order $y_1 \gg y_2 > z_1 > z_2 > \varepsilon > \Gamma > \gamma$, and we find that this ideal contains $\Gamma\gamma\varepsilon y_2^2(\Gamma - \gamma)(2\Gamma - \gamma)^2(\varepsilon - 2)$, so $y_2 = 0$. Finally, adding y_2 to the ideal yields that $0 = \Gamma y_1(\varepsilon - 1)(2\Gamma - \gamma)$, so the complete solution is

$$(y_1, y_2, z_1, z_2) = (0, 0, 0, 0).$$

We now consider the partial solution $z_2 = (\gamma - 2\Gamma)/(2\Gamma - 2\gamma)$. We compute a Gröbner basis $\mathcal{G}_2$ of I_2 with respect to the order $y_1 > y_2 \gg z_1 > z_2 > \varepsilon > \Gamma > \gamma$, and we find that the ideal contains $z_2\gamma(z_1 - z_2)^2$. Since this case was already studied, we may assume that $z_2 \neq 0$, so

$$z_1 = z_2 = \frac{\gamma - 2\Gamma}{2\Gamma - 2\gamma}.$$

Adding $z_1 - z_2$ to $\mathsf{sqfr}(\mathcal{G}_2)$ and computing a Gröbner basis for the order $y_1 \gg y_2 > z_1 > z_2 > \varepsilon > \Gamma > \gamma$, we find that the ideal contains $\gamma^2 y_2(\varepsilon - 1)P_{y_1}(2\Gamma - \gamma)$, so we have 2 new branches to consider. If $y_2 \neq 0$, then

$$y_1 = (1 - \varepsilon)y_2.$$

Otherwise, by adding $y_2 = 0$ to the system of equations, we find that the ideal contains $\gamma y_1^2 z_2$, so $y_1 = 0$, and in particular, this point is on $\{P_{y_1} = 0\}$.

□

5.3.3. *Locus of* $\{D = D' = 0\}$. From now, in section 5, many proofs are not given to clarify the presentation but may be found in [11].

Proposition 7. *The points of* $\{D = D' = 0\}$ *are given by:*

1. *the plane* $z_1 = z_2 = z_S$,
2. *the line* $y_1 = y_2 = 0$, $z_1 = z_2$,
3. *the surface (parameterized by* y_1, y_2*)*
$$z_1 = z_2 = \frac{\Gamma P_{y_2}^2(\gamma - 2\Gamma)}{2(\Gamma - \gamma)a_3},$$
with $a_3 = (\Gamma + \gamma)P_{y_1}^2 + \varepsilon(\varepsilon - 2)\Gamma(y_1 - y_2)(y_1 + y_2)$,
4. *the surface (parameterized by* y_1, z_2*)*
$$y_2 = \frac{y_1 z_2}{(1 - \varepsilon)z_1}, \quad z_1 = \frac{(2\Gamma - \gamma)z_2}{a_4},$$
with $a_4 = 2(\varepsilon - 2)(\Gamma - \gamma)\varepsilon z_2 + (2\Gamma - \gamma)(\varepsilon - 1)^2$,

5. *the surface (parameterized by y_2, z_2)*

$$z_1 = \frac{z_2 y_1}{(1-\varepsilon)y_2}, \quad y_1 = \frac{(1-\varepsilon)y_2\left((2\Gamma-\gamma)\Gamma y_2^2 + \gamma^2 z_2^2\right)}{a_5},$$

with $a_5 = \Gamma\left(2\varepsilon(\varepsilon-2)(\Gamma-\gamma)z_2 + (\varepsilon-1)^2(2\Gamma-\gamma)\right)y_2^2 + \gamma^2 z_2^2$.

5.3.4. *Equilibrium points.*

Lemma 5.1. *The equilibrium points associated to the vector field $X = DF - D'G$ are all contained in $\{D = D' = 0\}$.*

Linearization of the system at equilibrium points. For each of the components of the set of equilibrium points $\{D = D' = 0\}$ found in the previous paragraph, we inspect the behavior of the system in a neighborhood. Namely, for each equilibrium point q, we write

$$\frac{\mathrm{d}}{\mathrm{d}t}(q+\delta q) = (DF - D'G)(q) + A(q)\cdot\delta q + R(\delta q).$$

where $A(q) \coloneqq \mathrm{Jac}_q(DF - D'G)$, so that

$$\frac{\mathrm{d}}{\mathrm{d}t}(\delta q) = A(q)\cdot\delta q + R(q)(\delta q).$$

Here, Jac stands for the Jacobian. We can compute $A(q)$ explicitely: Indeed, recalling $X = DF - D'G$, then its first derivative is

$$\mathrm{d}X(q)(u) = \mathrm{d}D(q)(u)F(q) + D(q)\mathrm{d}F(q)(u) - \mathrm{d}D'(q)(u)G(q) - D'(q)\mathrm{d}G(q)(u), \tag{9}$$

so

$$A(q) = \nabla D(q)\cdot F(q) + D(q)\mathrm{Jac}_q(F)(q) - \nabla D'(q)\cdot G(q) - D'(q)\mathrm{Jac}_q(G)(q).$$

Now, we can examine the eigenvalue decomposition of $A(q)$ for each solution of proposition 7.

Solution 1. If $z_1 = z_2 = z_S = \frac{\gamma-2\Gamma}{2\Gamma-2\gamma}$, then the characteristic polynomial of A factors as

$$T^2\left(T - \gamma^2(2\Gamma-\gamma)^2(\varepsilon-1)P_{y_1}^2\right)^2.$$

The matrix $A(q)$ is diagonalizable.

Solution 2. If $y_1 = y_2 = 0$ and $z_1 = z_2$, the characteristic polynomial of $A(q)$ is T^4. The Jacobian matrix $A(q)$ can be trigonalized as

$$A(q) = P^{-1}\begin{bmatrix} 0 & 1 & 0 & 0 \\ 0 & 0 & 0 & 0 \\ 0 & 0 & 0 & 0 \\ 0 & 0 & 0 & 0 \end{bmatrix} P$$

with the transition matrix

$$P = \begin{bmatrix} 0 & 1 & -1 & 0 \\ \varepsilon\gamma^3(\varepsilon-1)(\varepsilon-2)z_1^2 P_{z_1} & 1 & 0 & 0 \\ 0 & 1 & 0 & 1 \\ \varepsilon\gamma^3(\varepsilon-1)(\varepsilon-2)z_1^2 P_{z_1} & 0 & 0 & 0 \end{bmatrix}.$$

Solution 3. If $z_1 = z_2 = \Gamma P_{y_2}^2(\gamma - 2\Gamma)/2(\Gamma - \gamma)a_3$, the characteristic polynomial of $A(q)$ factors as

$$T^2\left(T + \frac{b_3}{a_3}\right)\left(T - \frac{b_3}{a_3}\right)$$

with

$$b_3 = \Gamma\gamma^2(\varepsilon - 1)P_{y_1}P_{y_2}(2\Gamma - \gamma)^2.$$

The matrix $A(q)$ is diagonalizable.

Solution 4. If $y_2 = \frac{y_1 z_2}{(1-\varepsilon)z_1}$ and $z_1 = \frac{(2\Gamma-\gamma)z_2}{a_4}$, the characteristic polynomial of $A(q)$ factors as

$$T^2\left(T - \frac{b_4}{a_4}\right)\left(T + \frac{b_4}{a_4}\right)$$

with $b_4 = 2\varepsilon^2\gamma^3 z_2^3(\varepsilon-1)(\varepsilon-2)^2(2\Gamma-\gamma)(\Gamma-\gamma)P_{z_2}$. The matrix $A(q)$ is diagonalizable.

Solution 5. If $z_1 = \frac{z_2 y_1}{(1-\varepsilon)y_2}$ and $y_1 = \frac{(1-\varepsilon)y_2\left((2\Gamma-\gamma)\Gamma y_2^2+\gamma^2 z_2^2\right)}{a_5}$, the characteristic polynomial of $A(q)$ factors as

$$T^2\left(T - \frac{b_4(\Gamma y_2^2 + \gamma(z_2^2 + z_2))\Gamma y_2^2}{a_5}\right)^2.$$

The matrix $A(q)$ is diagonalizable.

5.3.5. *Special points.* There are two points at which A vanishes: the North Pole $N := (0,0,0,0)$ and $S := (0, z_S, 0, z_S)$. Both points are such that $D = D' = 0$, $\nabla D = \nabla D' = 0$, and additionally, at the North Pole, $F(N) = 0$. The North Pole is on solutions 2, 3, 4 and 5. The remainder at N is cubic:

$$\frac{\mathrm{d}}{\mathrm{d}t}(N + \delta q) = R(N)(\delta q) = O(\|\delta q\|^3).$$

The point S is the intersection of solutions 1 and 2. The remainder at S is quadratic. Let us now perform higher order studies for these special points.

Quadratic approximation at S. We study now the quadratic component $H_2 := Q(S)$ of the remainder $R(S)$:

$$\frac{\mathrm{d}}{\mathrm{d}t}(q + \delta q) = (DF - D'G)(q) + A(q)(\delta q) + Q(q)(\delta q) + O(\|\delta q\|^3),$$

with $\frac{\mathrm{d}q}{\mathrm{d}t}(S) = (DF - D'G)(S) = 0$ and $A(S) = 0$. We can compute Q by differentiating $X = DF - D'G$ again, as was done in [6, Sec. 3.4]. Differentiating (9) along q again, the second derivative of X is

$$\begin{aligned}\mathrm{d}^2X(q)(u,v) &= \mathrm{d}^2D(q)(u,v)F(q) + \mathrm{d}D(q)(u)\mathrm{d}F(q)(v) + \mathrm{d}D(q)(v)\mathrm{d}F(q)(u)\\ &\quad - \mathrm{d}^2D'(q)(u,v)G(q) - \mathrm{d}D'(q)(u)\mathrm{d}G(q)(v) - \mathrm{d}D'(q)(v)\mathrm{d}G(q)(u) \qquad (10)\end{aligned}$$

Note that second derivatives of F and G are 0, since their coordinates are affine in q. We wish to compute $H_2(\delta q) = Q(S)(\delta q, \delta q) = \frac{1}{2}\mathrm{d}^2X(q)(\delta q, \delta q)$. Since $\mathrm{d}D(S) = \mathrm{d}D'(S) = 0$, we find in the end that

$$H_2(\delta q) = h_2(\delta q)F(S) - h_2'(\delta q)G(S),$$

with

$$F(S) = \left(0, \frac{\gamma(2\Gamma-\gamma)}{2(\Gamma-\gamma)}, 0, \frac{\gamma(2\Gamma-\gamma)}{2(\Gamma-\gamma)}\right)^t, \quad G(S) = \left(\frac{\gamma}{2(\Gamma-\gamma)}, 0, \frac{(1-\varepsilon)\gamma}{2(\Gamma-\gamma)}, 0\right)^t,$$

and

$$h_2(\delta q) := \frac{1}{2}\mathrm{d}^2 D(S)(\delta q, \delta q) = (1-\varepsilon)(\delta z_1 - \delta z_2)(\delta z_1 - (1-\varepsilon)^2 \delta z_2)(2\Gamma-\gamma)\gamma^2,$$

$$h_2'(\delta q) := \frac{1}{2}\mathrm{d}^2 D'(S)(\delta q, \delta q) = (1-\varepsilon)(\delta z_1 - \delta z_2)(\delta y_2(\varepsilon-1) + \delta y_1)(2\Gamma-\gamma)^2\gamma^2.$$

Following [6] and [28], we study the projection of the differential equation $\dot{v} = H_2(v)$ on the sphere S^3. Let $w := v/\|v\|$ be this projection, it satisfies the differential equation

$$\begin{aligned}\dot{w} &= \frac{1}{\|v\|^2}\left(\dot{v}\|v\| - v\frac{\langle v, \dot{v}\rangle}{\|v\|}\right) = \frac{H_2(v)}{\|v\|} - \frac{\langle v, H_2(v)\rangle}{\|v\|^3} v \\ &= \|v\|\big(H_2(w) - \langle w, H_2(w)\rangle\, w\big)\end{aligned}$$

so we have to study the following differential equation on the sphere S^3:

$$\dot{v} = H_2(v) - \langle v, H_2(v)\rangle v =: H_2^\pi(v).$$

Invariants are related to the eigenvalues of the linearization of H_2^π at points where $H_2^\pi(v) = 0$. Those points are:

- lines of non-isolated singular points of H_2, that is vectors v such that $H_2(v) = 0$,
- ray solutions, that is vectors ξ such that there exists $\lambda \in \mathbb{R}\setminus\{0\}$, $H_2(\xi) = \lambda\xi$.

We study the linearization of H_2^π in some neighborhood of these solutions in S^3.

Proposition 8. *The blow-up at point S has no ray solution, and two sets of non-isolated singularities:*

1. *the projective plane $\delta z_1 = \delta z_2$;*
2. *the projective line $\delta y_2 = (1-\varepsilon)\delta y_1$, $\delta z_1 = (1-\varepsilon)^2\delta z_2$.*

In the first case, the Jacobian of the system is nilpotent. In the second case, it is diagonalizable with non-zero eigenvalues:

$$\frac{1}{2}\left(\bar{\delta y_2} + 1 \pm \sqrt{\bar{\delta y_2}^2 + (2\varepsilon-1)^2(\bar{\delta y_2}+1) - 4(\varepsilon-1)^4 - 2\bar{\delta y_2} + 1}\right),$$

where $\bar{\delta y_2} := \delta y_2/\delta z_1$.

Cubic approximation at N. We perform the same study at the North Pole N. With expression (10), we can verify that the quadratic component of $R(N)$ is 0. Indeed, $F(N) = 0$ and $\mathrm{d}^2 D'(N) = 0$. Further differentiating along q, we obtain

$$\begin{aligned}H_3(\delta q) &:= \frac{1}{6}\mathrm{d}^3 X(N)(\delta q, \delta q, \delta q) \\ &= \frac{1}{6}\left(3\mathrm{d}^2 D(N)(\delta q, \delta q)F(\delta q) - \mathrm{d}^3 D'(N)(\delta q, \delta q, \delta q)G(N)\right).\end{aligned}$$

Note that since we centered the coordinates at the North Pole, F is linear in q, so $\mathrm{d}F(q) = F$, and G is affine in q, so $\mathrm{d}G(q)$ is constant. As in the previous subsection, we study the projection of the differential equation $\dot{v} = H_3(v)$ on the sphere S^3, and its equilibrium points, which form lines of non-isolated singular points and ray solutions.

Proposition 9. *The cubic blow-up at the North Pole N, for admissible values of the parameters, has two sets of ray solutions:*

1. *the projective line*
$$\delta z_1 = \delta z_2 = 0, \quad (\varepsilon - 1)\delta y_1 + \delta y_2 = \frac{1}{\Gamma(2\Gamma - \gamma)\sqrt{1-\varepsilon}}, \tag{11}$$
2. *the quadric*
$$\delta y_1 = \delta y_2 = 0, \quad ((\varepsilon - 1)\delta z_1 - \delta z_2)^2 - (\varepsilon - 2)\delta z_1 \delta z_2 = \frac{1}{\gamma^3(2\Gamma - \gamma)(1-\varepsilon)},$$

and three sets of real non-isolated singularities:

1. *the plane*
$$\delta z_1 = \delta z_2, \quad \delta y_1(1-\varepsilon) = \delta y_2, \tag{12}$$
2. *the plane*
$$\delta y_2 = (1-\varepsilon)\delta y_1, \quad \delta z_2 = (1-\varepsilon)^2 \delta z_1, \tag{13}$$
3. *the surface defined by*
$$\begin{cases} 0 = \Gamma(\varepsilon-1)(2\Gamma-\gamma)\delta y_1^2 + (2\Gamma-\gamma)\Gamma\delta y_1\delta y_2 + \gamma^2(\varepsilon-1)\delta z_1^2 - \gamma^2(\varepsilon-1)\delta z_1\delta z_2, \\ 0 = \Gamma(\varepsilon-1)(2\Gamma-\gamma)\delta y_1\delta y_2 - \gamma^2\delta z_1\delta z_2 + (2\Gamma-\gamma)\Gamma\delta y_2^2 + \gamma^2\delta z_2^2, \\ 0 = \delta y_1\delta z_2 + (\varepsilon-1)\delta y_2\delta z_1. \end{cases}$$

For points on the line (11), the linearization of H_3^π is diagonal: the vectors $(1,0,0)$ and $(0,0,1)$ are eigenvectors, with the same eigenvalue, and the vector $(0,0,1)$ is in the kernel. For isolated singularities satisfying (12), the matrix is not diagonalizable, its Jordan form has the following structure:
$$\begin{bmatrix} 0 & 0 & 0 \\ 0 & * & 1 \\ 0 & 0 & * \end{bmatrix}.$$
For isolated singularities satisfying (13), the matrix is diagonalizable with 3 non-zero eigenvalues.

5.4. Singularity classification: non-exceptional case.

5.4.1. *Singularities of $\{\mathcal{D} = H_G = \{H_G, H_F\} = 0\}$.*

Proposition 10. *The set of singularities of $\{\mathcal{D} = H_G = \{H_G, H_F\} = 0\}$ is given, generically on authorized values of γ, Γ, by*

1. *the plane $z_1 = z_2 = z_S$;*
2. *the line $z_1 = z_2$, $y_1 = y_2 = 0$;*
3. *an irreducible variety of dimension 5.*

If $\gamma = \Gamma$, solution 2 becomes a surface defined by $z_1 = z_2$, $y_2 = (1-\varepsilon)y_1$.

5.4.2. *Locus of $\{\mathcal{D} = \mathcal{D}' = H_G = \{H_G, H_F\} = 0\}$.*

Proposition 11. *The solutions form the union of the hyperplane defined by*
$$z_1 = z_2 \tag{14}$$
and the hypersurface
$$y_1 = -\frac{y_2 P_{z_1}}{(\varepsilon - 1)\, P_{z_2}}. \tag{15}$$

5.4.3. *Equilibrium points.*

Lemma 5.2. *All equilibrium points associated to the vector field* $Z := \mathcal{D}\overrightarrow{H_F} - \mathcal{D}'\overrightarrow{H_G}$ *satisfying* $H_G = \{H_G, H_F\} = 0$ *are contained in* $\{\mathcal{D} = \mathcal{D}' = 0\}$.

Linearization of the system at equilibrium points. We consider the eigenvalue decomposition of the matrix

$$\mathcal{A} := \mathrm{Jac}(\mathcal{D}\overrightarrow{H_F} - \mathcal{D}'\overrightarrow{H_G})$$

at equilibrium points, given as the union of points satisfying Eq. (14) and (15).

Solutions of Eq. (14). If $z_1 = z_2$, the matrix $\mathcal{A}$ has rank 2, and its characteristic polynomial is

$$T^6\left(T^2 - \frac{\varepsilon(\varepsilon-1)(\varepsilon-2)\left(8(\Gamma-\gamma)^2 P_{y_1} y_1 y_2 + P_{z_2}(2\,P_{z_2}-\gamma)P_{y_2}\right)}{2P_{y_1}(\Gamma-\gamma)y_1}T + \left(\frac{(\varepsilon-1)\gamma P_{y_1}(2\Gamma-\gamma)}{y_1}\right)^2\right)$$

Solutions of Eq. (15). If $y_1 = -\frac{y_2 P_{z_1}}{(\varepsilon-1)P_{z_2}}$, the matrix $\mathcal{A}$ has rank 2, and its characteristic polynomial is

$$T^6\left(T^2 - 4\varepsilon y_2(\varepsilon-1)(\varepsilon-2)(\Gamma-\gamma)T + \left(\frac{2\gamma(z_1-z_2)(\varepsilon-1)^2(2\Gamma-\gamma)(\Gamma-\gamma)}{P_{z_1}}\right)^2\right).$$

The discriminant of the degree 2 factor factors as

$$\frac{16(\Gamma-\gamma)^2(\varepsilon-1)^2\left(a_6(z_1,y_2)-b_6(z_1,z_2)\right)\left(a_6(z_1,y_2)+b_6(z_1,z_2)\right)}{P_{z_1}^2}$$

with $a_6(z_1,y_2) = \varepsilon(\varepsilon-2)P_{z_1}y_2$, $b_6(z_1,z_2) = (2\Gamma-\gamma)(\varepsilon-1)\gamma(z_1-z_2)$, which induces the following classification of the eigenvalues of $\mathcal{A}$:

- if $|a(z_1,y_2)| > |b(z_1,z_2)|$: 2 single real eigenvalues;
- if $|a(z_1,y_2)| = |b(z_1,z_2)|$: 1 double real eigenvalue;
- if $|a(z_1,y_2)| < |b(z_1,z_2)|$: 2 single complex eigenvalues.

6. **Bi-saturation: first numerical results and LMI validation.** In this section, we use direct methods to compute candidates as minimizers and then we compare the cost with lower bounds given by LMI techniques. This process gives upper bounds on the gap between computed costs (obtained by the direct method) and the optimal cost, the cost being here the final time. If this gap is small then we can have good confidence on the global optimality of the candidate. On the other hand, if the gap is not so small, either the candidate is not optimal or the lower bound (given by the LMI technique) is not accurate enough. We roughly evaluate the confidence we can have on the lower bounds by solving first the mono-saturation problem and then the bi-saturation problem, since in the mono-saturation case, we have the optimal solutions, see theorem 3.6. The direct method is presented in section 6.1 while the LMI technique is detailed in section 6.2. Finally, the results are given in section 6.3.

6.1. **Direct approach (`Bocop`).** The `Bocop` [3] software implements a so-called direct transcription approach, where the continuous optimal control problem (OCP) is transformed into a nonlinear programming (NLP). The reformulation is done by a discretization of the time interval, with an approximation of the dynamics of the system by a generalized Runge-Kutta scheme. This is part of direct local collocation methods. We refer the reader to for instance [2], [19] and [31] for more details on direct transcription methods and NLP algorithms.

We present candidates as minimizers obtained by the `Bocop` software for the bi-saturation problem ($\mathrm{P_{BS}}$) in the Deoxygenated blood case (denoted C_1), the Oxygenated blood case (C_2) and the Cerebrospinal fluid case (C_3) with $\omega_{\max} = 2\pi \times 32.3$ and the Water case (C_4) with a larger value of $\omega_{\max}$. Let us mention that for C_4, the value of $\omega_{\max}$ is larger than $2\pi \times 32.3$ just to obtain a control law with longer bang arcs, to visualize better the solution. The parameter ε is fixed to 0.1 and let us recall that the associated relaxation times are given in Table 1. The time evolution of the state variables $q = (q_1, q_2)$ and of the control variable u are represented in Figs. 9 and 10 for cases C_1 and C_4 respectively (C_2 and C_3 are similar to C_1), while the optimal time is given in Table 2 and is compared with the optimal time for the saturation of a single spin. Note that for each case, there is one more Bang-Singular sequence (the first one) in the bi-saturation problem than in the mono-saturation case. Besides, the remaining part looks like the strategy to steer one single spin to the center of the Bloch ball, but for C_1, C_2 and C_3, the penultimate singular part of the trajectory do not follow exactly the horizontal lines $z_1 = z_2 = z_s = \gamma/(2\delta)$, $\delta = \gamma - \Gamma$. Finally, note that both spins reach the vertical line $y_1 = y_2 = 0$ with $z_1 = z_2$ at the beginning of the final singular arc (for which $u = 0$) in order to reach the center of the Bloch ball at the same time. In other words, the spins are synchronised at this time.

Case	Γ	γ	t_f (2 spins)	t_f (1 spin)
C_1	9.855×10^{-2}	$3.65\ \times10^{-3}$	44.769	42.685
C_2	2.464×10^{-2}	$3.65\ \times10^{-3}$	113.86	110.44
C_3	1.642×10^{-2}	2.464×10^{-3}	168.32	164.46
C_4	9.855×10^{-2}	9.855×10^{-2}	15.0237	8.7445

TABLE 2. Cases treated numerically corresponding respectively to the Deoxygenated case (C_1), the Oxygenated case (C_2), the Cerebrospinal fluid case (C_3) and the Water case (C_4). The 5th (resp. 4th) column gives the final time found by `Bocop` for the saturation of one spin (resp. two spins with B_1-inhomogeneity). The parameter ε is fixed to 0.1.

6.2. **LMI method (`GloptiPoly`).** A crucial step is to check whether the times presented in Table 2 and obtained with `Bocop` for the saturation problem are globally optimal using moment/LMI techniques. More precisely, these techniques provide for the saturation problem, lower bounds on the global optimal time which can be used as a validation of the global optimality if the gap between the lower bound obtained from moment/LMI techniques and the time obtained by the direct method is small. This combination of techniques has already been successful [8] in the contrast problem by nuclear magnetic resonance in medical imaging.

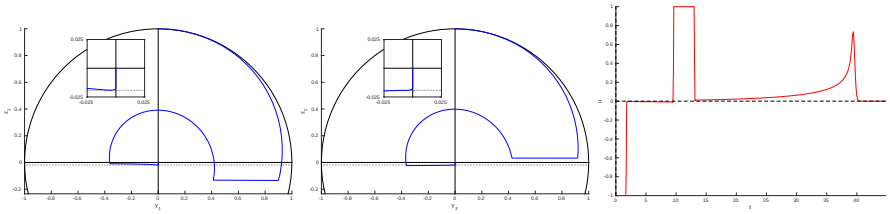

FIGURE 9. Deoxygenated blood case (C_1) with RF-inhomogeneity ($\varepsilon = 0.1$). Trajectories for spin 1 and 2 in the (y,z)-plane are portrayed in the first two subgraphs. The corresponding control is drawn in the right subgraph. The horizontal lines $z_1 = z_2 = z_s = \gamma/(2\delta)$, $\delta = \gamma - \Gamma$, is represented by dashed lines. Note that the last bang arc is not well captured by the direct solver because it is too short.

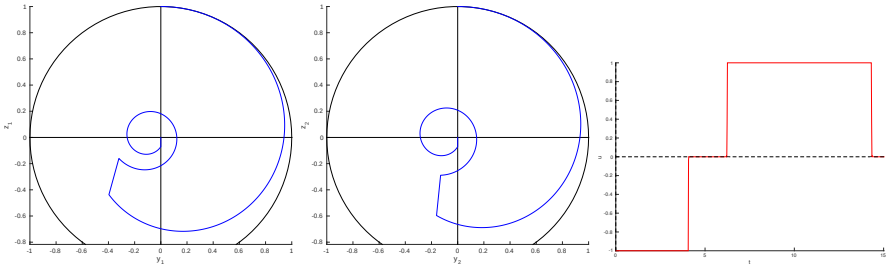

FIGURE 10. Water case (C_4) with RF-inhomogeneity ($\varepsilon = 0.1$). Trajectories for spin 1 and 2 in the (y,z)-plane are portrayed in the first two subgraphs.

The moment approach is a global optimization method which relaxes a non linear optimal control problem using measures as a linear programming (LP) problem. In the case where the data are polynomials, we can handle these measures by their moment sequences. Using powerful certificate coming from algebraic geometry, *e.g. Putinar's Positivstellensatz*, [33] this leads to an infinite dimensional LMI problem which can be truncated to a finite set of moments. The sequence of optimal values associated to these truncated problems converges to the optimal value of problem ($\mathrm{P_{BS}}$), that we denote by $T^*_{\min}$. We present a classical formulation and an alternative one which exploits the structure of the problem, based on [17]. Note that we present the method on the bi-saturation problem but it is straightforward to adapt the explanations for the mono-saturation problem.

Notations. B_n is the unit ball of dimension n, $\mathcal{M}^+(Z)$ is the set of finite, positive Borel measures supported on compact set Z and $\int f(z)\,d\mu$ denotes the integration of a continuous function $f \in C(Z)$ with respect to $\mu \in \mathcal{M}^+(Z)$.

6.2.1. *Step 1: linear program on measures.*

1st formulation: Moment approach using occupation measures. Following [26], the problem ($\mathrm{P_{BS}}$) can be embed into the linear program on measures:

$$
\begin{aligned}
T_{LP} &:= \inf_{\mu,\mu_f} \int \mathrm{d}\mu_f \\
&\text{s.t.} \int \left(\frac{\partial v}{\partial t} + \frac{\partial v}{\partial q}\,(F + u\,G) \right) \mathrm{d}\mu \\
&\qquad\qquad = \int v(\cdot, q_f)\,\mathrm{d}\mu_f - v(q_0), \quad \forall v \in \mathbb{R}[t,q], \\
&\mu \in \mathcal{M}^+([0,T] \times Q \times U), \quad \mu_f \in \mathcal{M}^+(Q_f),
\end{aligned} \tag{16}
$$

and where T is fixed, $Q_f := [0,T] \times \{(0,0,0,0)\}$, $Q := B_2 \times B_2$ are admissible state sets and $U := B_1$ is the admissible control set. Given any admissible pair $(q(\cdot), u(\cdot))$ for (P_{BS}), it corresponds a measure μ admissible for (16) achieving the same cost, hence $T^*_{\min} \geq T_{LP}$. Moreover, according to Theorem 3.6 (ii) of [26], there is no optimality gap and $T^*_{\min} = T_{LP}$.

Remark 7. Since the dynamic is autonomous, the time variable can be removed and the LP problem becomes

$$
\begin{aligned}
T_{LP} &= \inf_{\mu} \int \mathrm{d}\mu \\
&\text{s.t.} \int \frac{\partial v}{\partial q}\,(F + uG)\,\mathrm{d}\mu = v(q_f) - v(q_0), \quad \forall v \in \mathbb{R}[q], \\
&\mu \in \mathcal{M}^+(Q \times U).
\end{aligned} \tag{17}
$$

2nd formulation: Moment approach using modal occupation measures. In the first formulation (16) (respectively (17)), measures are supported on the set $[0,T] \times Q \times U$ (respectively $Q \times U$) of dimension $1 + 4 + 1 = 6$ (respectively 5) and we expect them to be located on the optimal trajectory $(q^*(\cdot), u^*(\cdot))$. An alternative formulation [17] is to model controls by measures such that the measures are supported on Q only. Indeed, note that the dynamic in (P_{BS}) is affine in the control u which takes its values inside the polytope $\mathrm{conv}\{-1,+1\}$. This optimal control problem can be written as a switching system with two modes, the first mode corresponding to $u = +1$ and the second mode corresponding to $u = -1$. This leads to consider

$$
\begin{aligned}
T_{LP'} &:= \inf_{\mu_1,\mu_2,\mu_f} \int \mathrm{d}\mu_f \\
&\text{s.t.} \quad \forall v \in \mathbb{R}[t,q], \int \left(\frac{\partial v}{\partial t} + \frac{\partial v}{\partial q}\,(F + G) \right) \mathrm{d}\mu_1 \\
&\quad + \int \left(\frac{\partial v}{\partial t} + \frac{\partial v}{\partial q}\,(F - G) \right) \mathrm{d}\mu_2 = \int v(\cdot, q_f)\,\mathrm{d}\mu_f - v(0, q_0), \\
&\mu_1, \mu_2 \in \mathcal{M}^+([0,T] \times Q), \quad \mu_f \in \mathcal{M}^+(Q_f)
\end{aligned} \tag{18}
$$

where T is fixed.

6.2.2. *Step 2: Moment SDP.* An important feature of the problems (16)-(18) is their algebraic structure: the dynamic is polynomial and the sets Q and U are compact basic semi-algebraic sets. In these settings, it is possible to handle the measures by their moments which leads to a semi-definite program on countably many moments. Let us introduce for a multi-index $\alpha := (\alpha_1, \ldots, \alpha_p) \in \mathbb{N}^p$ and $y := (y_1, \ldots, y_p) \in \mathbb{R}^p$, the notation $|\alpha|_1 := \sum_{i=1}^p \alpha_i$ and y^α which stands for the monomial $y_1^{\alpha_1} \ldots y_p^{\alpha_p}$. Then, we denote by $\mathbb{N}^p_d$ the set $\{\alpha \in \mathbb{N}^p \mid |\alpha|_1 \leq d\}$.

Definition 6.1. The moment of order $\alpha \in \mathbb{N}^p$ of a measure μ supported on $Z \subset \mathbb{R}^p$ is the real $y_\alpha := \int z^\alpha \, \mathrm{d}\mu$. Besides, $\mu \in \mathcal{M}(Z)$ is said to be a representing measure for a sequence $(y_\alpha)_\alpha$ if $y_\alpha = \int z^\alpha \, \mathrm{d}\mu$ for all $\alpha \in \mathbb{N}^p$.

Definition 6.2. Given an arbitrary sequence of reals $(y_\alpha)_\alpha$, we define the Riesz linear functional $l_y \colon \mathbb{R}[z] \to \mathbb{R}$ by $l_y(z^\alpha) := y_\alpha$ for all $\alpha \in \mathbb{N}^p$.

Definition 6.3. The moment matrix $M_d(y)$ of order d is such that $l_y(p(z)^2) = p' M_d(y) p$ for all polynomials $p(z)$ of degree d whose coefficients are denoted by the vector p. In particular, the (i,j)th entry is $M_d(y)[i,j] = l_y(z^{i+j}) = y_{i+j}$, $\forall i,j \in \mathbb{N}^p_d$.

Similarly, the localizing matrix of order d associated with a sequence (y_α) and a polynomial $g(z)$ is the matrix $M_d(g\,y)$ such that $l_y(g(z)\,p(z)^2) = p' M_d(g\,y) p$ for all polynomial $p(z)$ of degree d.

Proposition 12. *Let Z be a compact basic semi-algebraic set defined by $Z := \{z \in \mathbb{R}^p \mid g_k(z) \geq 0,\, k = 1, \dots, n_Z\}$. Then, a necessary condition for a sequence $(y_\alpha)_\alpha$ to have a representing measure $\mu \in \mathcal{M}^+(Z)$ is*

$$M_d(y) \succeq 0, \quad M_d(g_k\, y) \succeq 0, \quad \forall d \in \mathbb{N}, \forall k = 1, \dots, n_Z.$$

Finally, we introduce

$$\begin{aligned}[0,T] \times Q \times U = &\{(t,q,u) \mid q = (q_{11}, q_{12}, q_{21}, q_{22}),\, g_1(t,q,u) := t(T-t) \geq 0,\\ &g_2(t,q,u) := 1 - q_{11}^2 - q_{12}^2 \geq 0,\; g_3(t,q,u) := 1 - q_{21}^2 - q_{22}^2 \geq 0,\\ &g_4(t,q,u) := 1 - u^2 \geq 0\},\end{aligned}$$

and

$$\begin{aligned}Q_f = \{(t,q) \in \mathbb{R}^5 \mid &g_0^f(t) := t(T-t) \geq 0,\, g_1^f(q) := q_{11} = 0,\\ &g_2^f(q) := q_{12} = 0,\, g_3^f(q) := q_{21} = 0,\, g_4^f(q) := q_{22} = 0\}.\end{aligned}$$

We denote by l_{y^μ}, $l_{y^{\mu_f}}$ the Riesz functionals associated respectively with the sequences y^μ and y^{μ_f}. Then, the moment SDP problem associated with (16) is

$$\begin{aligned}T_{SDP} := &\inf_{y^\mu,\, y^{\mu_f}} l_{y^{\mu_f}}(1)\\ &l_{y^\mu}\left(\frac{\partial v}{\partial t} + \frac{\partial v}{\partial q}(F + uG)\right) = l_{y^{\mu_f}}(v(\cdot, q_f)) - v(0, q_0), \quad \forall v \in \mathbb{R}[t,q],\\ &M_d(y^\mu) \succeq 0,\; M_d(g_i\, y^\mu) \succeq 0,\; i = 1 \dots 4,\; \forall d \in \mathbb{N},\\ &M_d(y^{\mu_f}) \succeq 0,\; M_d(g_i^f\, y^{\mu_f}) \succeq 0,\; i = 0 \dots 4,\; \forall d \in \mathbb{N}.\end{aligned} \tag{19}$$

At the end, according to Proposition 12, we have $T_{LP} \geq T_{SDP}$ and this is in fact an equality according to Theorem 3.8 from [25].

6.2.3. *Step 3: Hierarchy of SDP problems.* Note that $M_{d+1}(y) \succeq 0$ implies $M_d(y) \succeq 0$. The LMI constraints and the sequences (y^μ_α),$(y^{\mu_f}_\alpha)$,(y^μ_α) of (19) are truncated which lead to $r \geq 1$ to the Lasserre's hierarchy parameterized by $r \geq 1$:

$$\begin{aligned}T^r_{LMI} := &\inf_{(y^\mu_\alpha)_{|\alpha| \leq 2r},\, (y^{\mu_f}_\alpha)_{|\alpha| \leq 2r}} l_{y^{\mu_f}}(1)\\ &l_{y^\mu}\left(\frac{\partial v}{\partial t} + \frac{\partial v}{\partial q}(F + uG)\right) = l_{y^{\mu_f}}(v(\cdot, q_f)) - v(0, q_0), \quad \forall v \in \mathbb{R}[t,q],\\ &M_r(y^\mu) \succeq 0,\; M_{r-s_i}(g_i\, y^\mu) \succeq 0,\; i = 1 \dots 4\\ &M_r(y^{\mu_f}) \succeq 0,\; M_r(g_i^f\, y^{\mu_f}) \succeq 0,\; i = 0 \dots 4.\end{aligned} \tag{20}$$

where $s_i = \deg(g_i)/2$ if $\deg(g_i)$ is even and $s_i = (\deg(g_i)+1)/2$ otherwise. The main result is then the following.

Theorem 6.4 (Theorem 5.6, [25]). *We have*

$$T^*_{\min} = T_{LP} = T_{SDP} \geq \ldots \geq T^{r+1}_{LMI} \geq T^r_{LMI} \geq \ldots \geq T^1_{LMI}.$$

Moreover the sequence of lower bounds $(T^r_{LMI})_r$ *converges to* $T^*_{\min}$ *as* $r \to \infty$.

6.2.4. *Summary of the LMI method.* The moment/LMI method approach for optimization consist in reformulating an optimization problem as a linear program on measures. When the data is polynomial, a hierarchy of LMI relaxations can be constructed, whose costs converge to that of the original problem. The strong feature of the method is that those LMI generate lower bounds on the true cost, and can therefore be used as certificates of global optimality. On the other hand, the weak points of the method are its poor algorithm complexity for unstructured problem, as well as for the special case of optimal control, the unavailability of a generic method to recover controls. Note that the passage to a given LMI relaxation starting from measure problem (16) or (18) can be fully automated with high-level commands using the `GloptiPoly` [20] toolbox.

6.3. **Validation of the numerical results.** The problem (20) corresponds to the multisaturation problem of two spins associated with the LP problem (16). Likewise, we can construct from the LP problem (18) a hierarchy of LMI relaxations parameterized by r in the single spin case and the two spins case to compare the two formulations. We use the `Mosek` [30] toolbox to solve the SDP problems. Let t_f denote the best solution found with the `Bocop` software, given in Table 2 for the single spin case and the two spins case. The value of the parameters for (20) are: $\varepsilon = 0.1$, $q_0 = (0,1,0,1)$, $q_f = (0,0,0,0)$ and $T = t_f$. The lower bounds of T^*_{min} are T^r_{LMI} (resp. $T^r_{LMI'}$) associated with the LP problem (16) (resp. (18)) and are given in Table 3. Introducing $n := \dim Q$, $m := \dim U$ and $n_d := 2$ the number of modes for the second formulation, then at the relaxation order d, the number of moments (see Table 3) involved in the SDP problem associated with (16) and (18) is given by

$$N_m := \binom{n+m+1+2d}{n+m+1} + \binom{n+1+2d}{n+1}$$

and

$$N_m := (n_d+1)\binom{n+1+2d}{n+1}$$

respectively.

In Fig. 11 are represented the relative error $\mathrm{err}(r) := (t_f - T^r_{LMI})/t_f$ for the cases C_1, C_2, C_3 and C_4, where T^r_{LMI} is the optimal value of (20) in the single spin case and the two spins case. Note that in the single spin case, we know the structure and the optimal value of the global solution and we can compute the numerical gap between the direct approach and the moment/LMI approach.

Both formulations are computationally demanding, the relative errors on the final times found by `Bocop` for the cases C_2, C_3, C_4 are less than 5% for the single spin saturation and less than 10% for the multisaturation. Note that these two formulations have to be compared not only on the sharpness of the lower bounds but also considering the number of moments involved in the hierarchy.

	1st Formulation		2nd Formulation	
r	N_m	$(t_f - T^r_{LMI})/t_f$	N_m	$(t_f - T^r_{LMI'})/t_f$
1	25	0.8143	30	0.818
2	105	0.5164	105	0.5958
3	294	0.2611	252	0.4355
4	660	0.1491	495	0.1842
5	1287	0.0932	858	0.1284
6	2275	0.0643	1365	0.096
7	3740	0.0517	2040	0.0797
8	5814	0.0461	2907	0.0716

TABLE 3. Single spin saturation for the case C_2. T^r_{LMI} is the optimal value of the hierarchy (20). Likewise, $T^r_{LMI'}$ is the optimal value of the hierarchy of SDP problems derived from (18). $t_f = 110.44$ is the best time found by the `Bocop` software. The second and fourth columns are the relative errors between best solution found by the `Bocop` software and the one found by moment/LMI techniques for each relaxation order r.

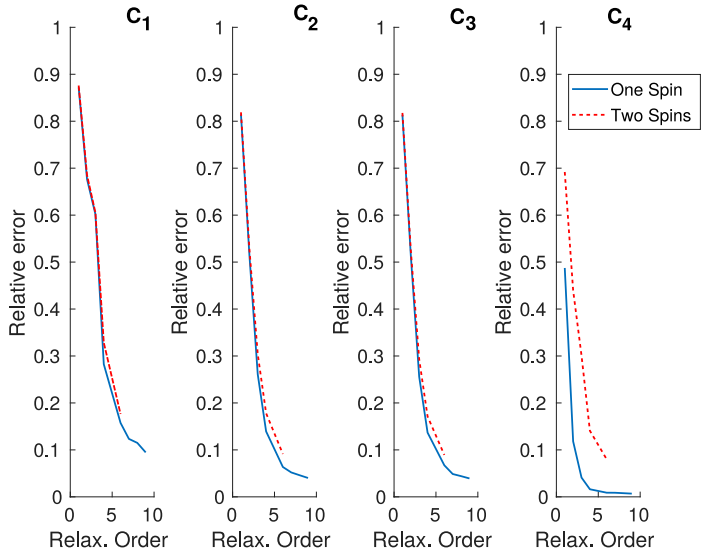

FIGURE 11. Saturation problem of one spin and two spins for the cases C_1, C_2, C_3 and C_4. Relative error $\mathrm{err}(r) = (t_f - T^r_{LMI'})/t_f$ where r is the order of relaxation, $T^r_{LMI'}$ is the optimal value of (20) using the formulation (18) and t_f is the final time computed with `Bocop`.

7. **Bi-saturation: influence of the relaxation parameters and homotopy.** We use a combination of multiple shooting and differential path following methods to analyze the influence of the parameters on BC-extremals from problem ($\mathrm{P_{BS}}$). We recall the multiple shooting technique in section 7.1, we give some details about homotopy and monitoring in section 7.2 and we present the results in section 7.3.

For the numerical results we fix ε and $\gamma^2+\Gamma^2$ and we present three different solutions which emphasize the complex structure of the singular flow, analyzed in section 5.

7.1. **Multiple shooting (`HamPath`).** Since the optimal structures are composed of sequences of bang and singular arcs, we must use multiple shooting instead of single shooting. We refer to [15, 29] for details about multiple shooting algorithms and to [8, 9] for explanations about multiple shooting in the context of medical imaging. One particularity is that the solutions end with a singular arc and not a bang arc, contrary to the examples given in [29]. Because of that, the shooting equations are more intricate as we can see it hereinafter.

Let $u_s(x,p)$ denote the singular control and $u_\pm := \pm u_{\max} = \pm 1$ the positive and negative bang controls. Let us assume we have a solution with a structure of the form BSBS, *i.e.* Bang-Singular-Bang-Singular. We note the unknowns of the shooting function $y := (p_0, t_f, t_1, t_2, t_3, z^1, z^2, z^3)$ and the shooting function is given by:

$$
\begin{array}{llll}
S\colon & \mathbb{R}^{32} & \longrightarrow & \mathbb{R}^{32} \\
 & y = \begin{bmatrix} p_0 \\ t_f \\ t_1 \\ t_2 \\ t_3 \\ z^1 \\ z^2 \\ z^3 \end{bmatrix} & \longmapsto & S(y) := \begin{bmatrix} u_\pm H_1(z^0) + p^0 \\ H_1(z^1) \\ H_{01}(z^1) \\ H_1(z^3) \\ H_{01}(z^3) \\ y_2(t_f, t_3, z^3, u_s) \\ z_2(t_f, t_3, z^3, u_s) \\ (p_{z_1}(t_f, t_3, z^3, u_s) + p_{z_2}(t_f, t_3, z^3, u_s))\gamma + p^0 \\ z(t_1, 0, z^0, u_\pm) - z^1 \\ z(t_2, t_1, z^1, u_s) - z^2 \\ z(t_3, t_2, z^2, u_\pm) - z^3 \end{bmatrix}
\end{array}
$$

where $p^0 = -1$ in the normal case, where $z^0 := (q_0, p_0)$ is the initial state-costate vector with $q_0 = (0,1,0,1)$. To get a BC-extremal we want to solve the shooting equations

$$S(y) = 0.$$

The first equation comes from the fact that the final time is free (and the Hamiltonian is constant along extremals so we can impose its value at the initial time), the four following equations means that the associated extremal becomes singular at z^1 and z^3. The last three *matching* equations improve numerical stability. Note that we have only three equations (the three remaining equations) associated to the final condition: $q(t_f) = (0,0,0,0)$. This is because we can find a redundant equation and this is due to the fact that the trajectory ends with a singular (and not bang) arc. Indeed, the fact that $H_1(z^3) = H_{01}(z^3) = 0$ implies that $H_1(z(t_f, t_3, z^3, u_s)) = H_{01}(z(t_f, t_3, z^3, u_s)) = 0$. But, if $(p_{y_1}(t_f, t_3, z^3, u_s), p_{z_1}(t_f, t_3, z^3, u_s)) \neq 0$, then

$$
\left.\begin{aligned}
H_1(z(t_f, t_3, z^3, u_s)) &= 0 \\
H_{01}(z(t_f, t_3, z^3, u_s)) &= 0 \\
y_2(t_f, t_3, z^3, u_s) &= 0 \\
z_2(t_f, t_3, z^3, u_s) &= 0 \\
(p_{z_1}(t_f, t_3, z^3, u_s) + p_{z_2}(t_f, t_3, z^3, u_s))\gamma + p^0 &= 0
\end{aligned}\right\} \quad \Rightarrow \quad \begin{aligned} & y_1(t_f, t_3, z^3, u_s) = \\ & z_1(t_f, t_3, z^3, u_s) = 0. \end{aligned}
$$

Hence, for any zero of the shooting function, the associated trajectory reaches the target $q_f = (0,0,0,0)$ at the final time if $(p_{y_1}(t_f, t_3, z^3, u_s), p_{z_1}(t_f, t_3, z^3, u_s)) \neq 0$. Let us recall that one difficulty to solve a shooting equation is to have a good initial guess. To determine the structure and make the shooting method converge, we use direct methods from the `Bocop` software. This combination of direct and indirect methods has already been successful [8] in the contrast problem by nuclear magnetic resonance in medical imaging.

7.2. **Homotopy and monitoring.** Once we have a solution obtained by a multiple shooting method, we can use differential homotopy [1] techniques to study the deformation of the solution with respect to the relaxation parameters. The homotopy method, from `HamPath` [16] software, is based on a Predictor-Corrector algorithm with a high order and step-size control Runge-Kutta scheme for the prediction and with a classical simplified Newton method for the correction. We combine the differential path following method with monitoring at each accepted step of the integration to detect if structural changes occur during the homotopy. We consider three different monitoring for which we give the associated action for the saturation problem:

- check if each arc (except the first and the last arcs) has positive length, that is if $t_i \leq t_{i+1}$. If not, the arc with negative length has to be removed.
- check if the singular control on each singular arc (except the last arc because it is 0) is admissible. If not, one bang arc has to be added.
- check if the switching function on each bang arc remains of constant sign. If not, one singular arc has to be added.

Let us illustrate the third monitoring on an example. We write $\Gamma = \rho\cos\theta$ and $\gamma = \rho\sin\theta$, and we consider an homotopy (called H1a) on θ with $\rho =: \bar{\rho} \approx 0.0551$, from $\theta =: \theta_{\max} = \operatorname{atan}(2) \approx 1.1071$ to $\theta =: \theta_{\min} = 0.02$. One starts from $\theta = \theta_{\max}$ with a structure of the form BSBS ($\sigma_-\sigma_s\sigma_+\sigma_0$) where σ_0 is a singular arc associated to a zero singular control. Around $\theta =: \theta_{1\mathrm{a},1} \approx 0.5069$, the monitoring detects a change in the structure. Let us denote by $\theta^+_{1\mathrm{a},1} \geq \theta_{1\mathrm{a},1} \geq \theta^-_{1\mathrm{a},1}$ the two values of θ at the two consecutive steps such that these inequalities are satisfied. Since, for $\theta = \theta^-_{1\mathrm{a},1}$, the switching function crosses 0 two times on the first bang arc, one has to stop the homotopy and add a singular arc, see figure 12.

7.3. **Numerical results.**

7.3.1. *Methodology.* We write $\Gamma = \rho\cos\theta$ and $\gamma = \rho\sin\theta$, and we consider only homotopies on θ with $\rho = \bar{\rho} \approx 0.0551$. This particular value of ρ is such that we retrieve the fat case, that is $T_1 = 0.2$ and $T_2 = 0.1$, with $u_{\max} = 1$ and $\omega_{\max} = 2\pi \times 32.3$, this specific value of $\omega_{\max}$ being excerpted from [10]. We present some results for a range of values of θ to illustrate the role of this parameter on the structure of some BC-extremals from problem (P_{BS}). The value of θ ranges between $\theta = \theta_{\max} = \operatorname{atan}(2) \approx 1.1071$ and $\theta = \theta_{\min} = 0.02$. The maximal bound is chosen to satisfy the physical constraint $0 < \gamma \leq 2\Gamma$ while the minimal bound is chosen to include all the practical cases, see Table 1. The saturation of a pair of spins is a much more complex problem than the mono-saturation, so we do not intend to get any optimal synthesis but just optimal trajectories to steer both spins from the North Pole to the center of the Bloch ball in minimum time and in a synchronized fashion. Besides, we just analyze the influence of θ for fixed values of $\rho = \bar{\rho}$ and $\varepsilon = 0.1$.

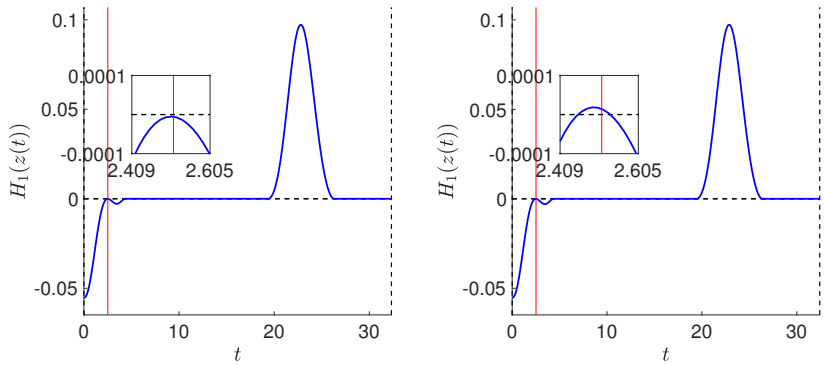

FIGURE 12. The relaxation parameters are given by $\rho = \bar{\rho}$ and (Left) $\theta = \theta^+_{1a,1}$, (Right) $\theta = \theta^-_{1a,1}$. Each subgraph represents the graph of the switching function H_1 along the extremal. For $\theta = \theta^-_{1a,1}$, we observe that H_1 crosses 0 twice. A singular arc must be added to continue the homotopy on θ. A zoom in on the graph of H_1 is given and may be located thanks to the vertical red lines. Note that we add a singular arc, since in this case the singular extremal is time-minimizing for small time.

The methodology is the following. For a given initial value of θ, we use direct method to determine the structure and to initialize the multiple shooting method. Then, we perform homotopies on θ with monitoring to stop it if necessary. If a change in the structure is detected, then, we update the multiple shooting function and continue the homotopy until we reach the final value of θ if possible. Note that in the multi-saturation problem, there exist many local solutions. Thus, for a given value of θ we must compare the cost of each solution. This leads to compute several path of zeros and then compare them in terms of cost. We choose to present four different paths, see Table 4 and Fig. 13. Note that the paths of zeros are computed with a very good accuracy according to the bottom-right subgraph of Fig. 13. The details are given in section 7.3.3 while we present some particular cases in the next section.

7.3.2. *Particular cases.* Before we give some details about the homotopies, we present three particular cases excerpted from these homotopies: the Water case ($\omega_{\max} = 10.2684$), the Fat case ($\omega_{\max} = 202.9469 \approx 2\pi \times 32.3$) and the Cerebrospinal Fluid case ($\omega_{\max} = 61.1840$). See Table 1 for the corresponding values of θ. All the others cases have the same optimal structure than the Cerebrospinal Fluid case. One can see from Fig. 13-14 that for the Water case, the optimal structure is of the form $\sigma_-\sigma_s\sigma_+\sigma_0$ and the solution is given by the homotopie (H1a). The solution is given on Fig. 14. For the Fat case, the structure is of the form $\sigma_-\sigma_s\sigma_-\sigma_s\sigma_+\sigma_0$ and it is also given by (H1a), see Fig. 15. Finally, for the Cerebrospinal Fluid case, the structure is of the form $\sigma_-\sigma_s\sigma_+\sigma_s\sigma_+\sigma_0$ and it is given by (H1b), see Fig. 16. One can notice different interactions between bang and singular arcs depending on the case, and one can see that the horizontal line $z = z_s = \gamma/(2\delta)$ plays a crucial role in the optimal trajectory when it intersects the Bloch ball.

7.3.3. *Details on the homotopies.* Let us give now some details about the different homotopies. The first two paths (called H1a and H1b) are interesting since, even

Name	Init	Transition	End
H1a	$\theta_{\max} \approx 1.1071$ $\sigma_-\sigma_s\sigma_+\sigma_0$	$\theta_{1a,1} \approx 0.5069$ $\sigma_-\sigma_s\sigma_-\sigma_s\sigma_+\sigma_0$	$\theta_{1a,2} \approx 0.2722 > \theta_{\min} = 0.02$ $\sigma_-\sigma_s\sigma_-\sigma_+\sigma_0$
H1b	$\theta_{\min}$ $\sigma_-\sigma_s\sigma_+\sigma_s\sigma_+\sigma_0$	$\theta_{1b,1} \approx 0.2752$ $\sigma_-\sigma_s\sigma_+\sigma_0$	$\theta_{1b,2} \approx 0.3018 < \theta_{\max}$ $\sigma_-\sigma_s^-\sigma_+\sigma_0$
H2	$\theta = 0.2$ $\sigma_+\sigma_s\sigma_+\sigma_s\sigma_+\sigma_0$	$\theta_{2,1} \approx 0.3618$ $\sigma_+\sigma_s\sigma_+\sigma_0$	$\theta = \mathrm{atan}(1.5) \approx 0.9828$ $\sigma_+\sigma_s\sigma_+\sigma_0$
H3	$\theta = 0.25$ $\sigma_+\sigma_s\sigma_+\sigma_s\sigma_+\sigma_0$	$\theta_{3,1} \approx 0.4778$ $\sigma_+\sigma_s\sigma_+\sigma_0$	$\theta = \theta_{\max}$ $\sigma_+\sigma_s\sigma_+\sigma_0$

TABLE 4. The homotopies are detailed on each line. The first column gives the name of the homotopy. The second colum "Init" gives the initial value of θ, the associated structure with the reference to the figure which presents the trajectory with the control and the switching function. For this initial value, the solution is obtained from direct method and multiple shooting. The column "Transition" gives the same details but when a first change in the structure is detected during the homotopy thanks to the monitoring. The last column "End" gives again the same details at the end of the homotopy. For the homotopies H1a and H1b, the end occurs when a second change in the structure is detected while for H2 and H3, the end occurs when the final value of θ is reached. The red and green colors may help to understand the change in the structure, which is explained more in details in this section.

if they are distinct paths (see bottom-left subgraph of Fig. 13), they intersect in terms of cost for a value $\theta^* \in [\theta_{1b,1}, \theta_{1b,2}]$, where we introduce $\theta_{1b,1} \approx 0.2752$ and $\theta_{1b,2} \approx 0.3018$. For $\theta \leq \theta^*$, H1b is better and for $\theta \geq \theta^*$, H1a is better, see top-left subgraph of Fig. 13. The homotopy H1a has been already introduced in section 7.2. One starts from $\theta = \theta_{\max}$ with a structure of the form BSBS ($\sigma_-\sigma_s\sigma_+\sigma_0$). Around $\theta = \theta_{1a,1} \approx 0.5069$, the monitoring detects a change in the structure: a singular arc has to be added inside the first negative bang arc and the structure becomes $\sigma_-\sigma_s\sigma_-\sigma_s\sigma_+\sigma_0$. A new change occurs around $\theta =: \theta_{1a,2} \approx 0.2722$: the second singular arc vanishes and the structure becomes $\sigma_-\sigma_s\sigma_-\sigma_+\sigma_0$. We stop the homotopy here since the homotopy H1b is better for this value of θ. Le us explain the homotopy H1b: this homotopy starts from $\theta = \theta_{\min}$ with a structure of the form BSBSBS ($\sigma_-\sigma_s\sigma_+\sigma_s\sigma_+\sigma_0$). A first change in the structure is detected around $\theta =: \theta_{1b,1} \approx 0.2752$: the second singular arc vanishes and the structure becomes $\sigma_-\sigma_s\sigma_+\sigma_0$. A second change occurs around $\theta =: \theta_{1b,2} \approx 0.3018$: the control saturates at the end of the first singular arc. We denote by σ_s^- this singular arc with since at the end the control takes the value -1. The structure is now $\sigma_-\sigma_s^-\sigma_+\sigma_0$ and we do not continue the homotopy since H1a is better for $\theta = \theta_{1b,2}$. The different structures with the names of the homotopies and the associated figures to observe the trajectories and the control are given in Table 4.

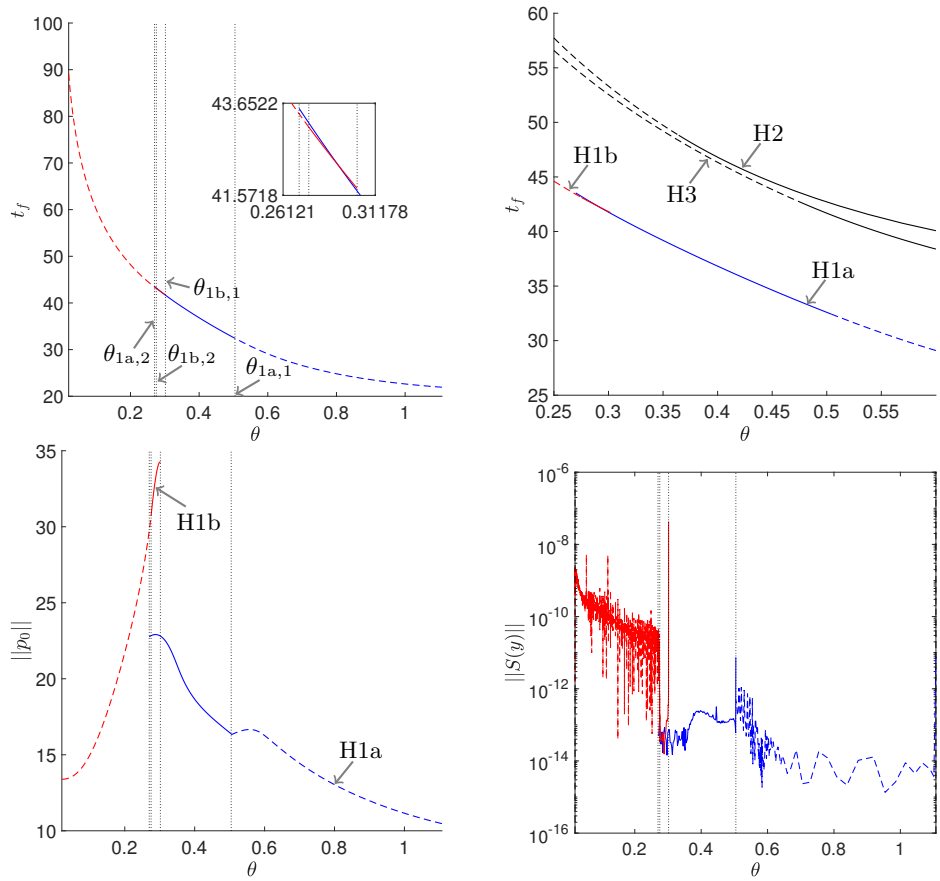

FIGURE 13. The homotopies H1a, H1b, H2 and H3 are presented respectively in blue, red, black and black. The homotopies H2 and H3 are presented only on the top-right subgraph. The plain and dashed lines distinguish the different structures. The top-left subgraph gives the cost (*i.e.* the final time t_f) with respect to θ for the homotopies H1a and H1b. One can see (it is more visible in the zoom) the intersection of the two paths of zeros in terms of cost. H1b is better for small value of θ and H1a is better for greater values. One can notice that this two paths of zeros are distinct from the bottom-left subgraph. This subgraph gives the norm of the initial adjoint vector with respect to the homotopic parameter. The norm of the shooting function along the paths H1a and H1b is given in the bottom-left subgraph.The strategies from H1a and H1b are compared with homotopies H2 and H3 on the top-right subgraph.

Let us give some details about the two last homotopies. The homotopy H2 starts with a local solution (not globally optimal, see top-right subgraph of Fig. 13) of the form $\sigma_+\sigma_s\sigma_+\sigma_s\sigma_+\sigma_0$ for $\theta = 0.2$. This solution has the particularity that all the bang arcs are positive bang arcs. Besides, the trajectory (see Fig. 17) has a

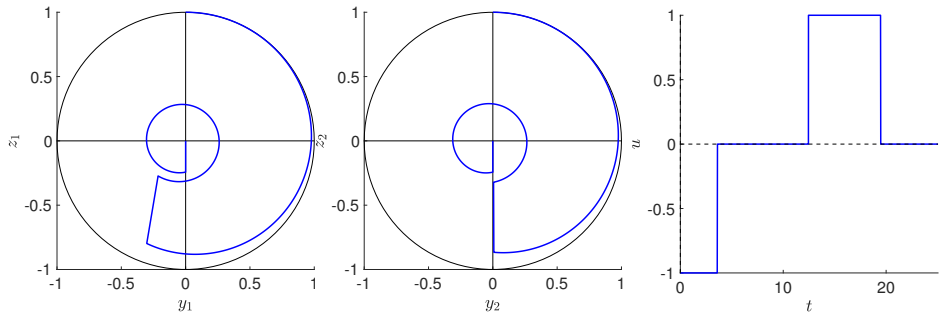

FIGURE 14. Water case: $\rho = \bar{\rho}$, $\theta = 0.7854$ and $\varepsilon = 0.1$. Trajectories of spins 1 and 2, and control.

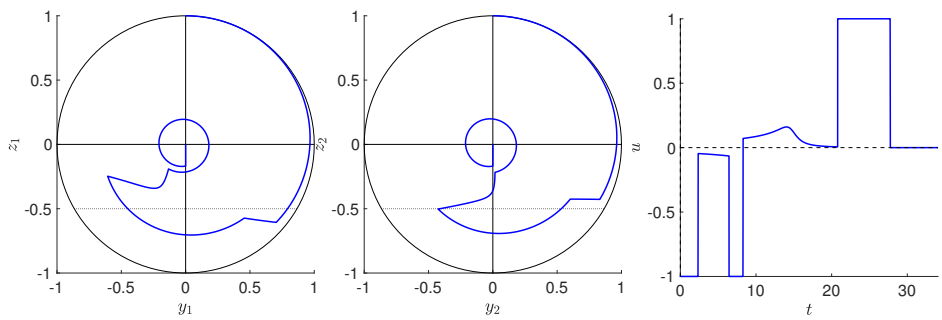

FIGURE 15. Fat case: $\rho = \bar{\rho}$, $\theta = 0.4636$ and $\varepsilon = 0.1$. Trajectories of spins 1 and 2, and control.

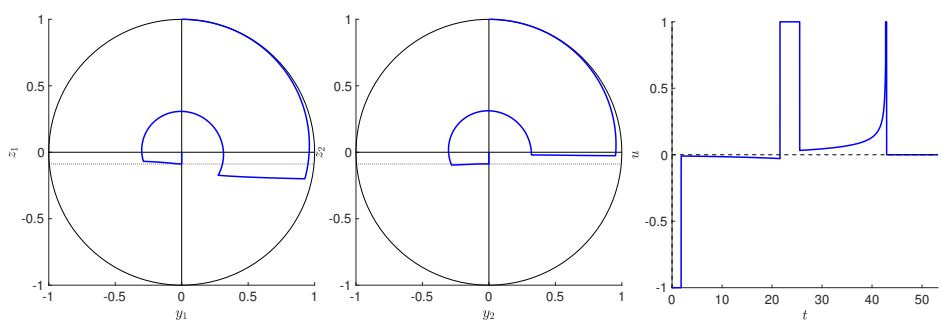

FIGURE 16. Fluid case: $\rho = \bar{\rho}$, $\theta = 0.1489$ and $\varepsilon = 0.1$. Trajectories of spins 1 and 2, and control.

self-intersection which prevents the BC-extremal to be globally optimal. During the homotopy there is only one change, the first singular arc vanishes around $\theta =: \theta_{2,1} \approx 0.3618$. This homotopy may be compared with the homotopy H3. The homotopy H3 is similar as H2 but the last bang arc is longer. During this last bang arc, the trajectory realizes a complete turn around its center. There is also one single change around $\theta =: \theta_{3,1} \approx 0.4778$, from which the first singular arc vanishes.

8. **Conclusion.** In this article we made a complete use of the state of the art in geometric, symbolic and numerical techniques to analyze the problem of saturating a pair of spins in relation with the B_1-inhomogeneities, that is inhomogeneities of

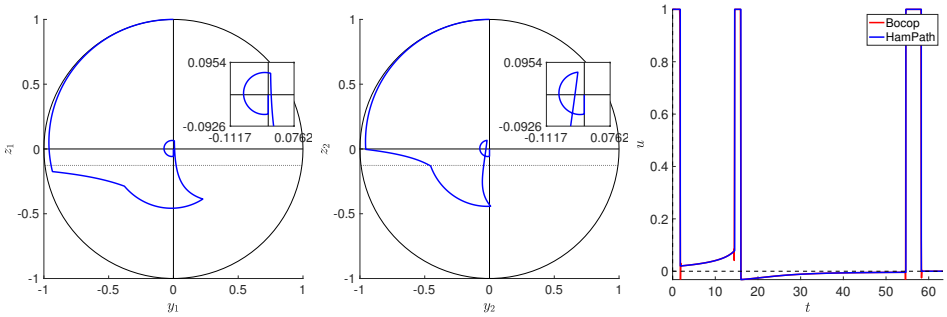

FIGURE 17. H2: $\rho = \bar{\rho}$, $\theta = 0.2$ and $\varepsilon = 0.1$. Trajectories of spins 1 and 2, control and H_1.

the applied RF-field. We extend the results in many directions. First of all, the time minimal syntheses for a single spin are classified, taking into account the relaxation parameters and the control bounds. For a pair of spins, the crucial theoretical problem is to classify the singularities of the extremal flow. This is realized using symbolic computations based on Gröbner basis to compute the singularities of the flow and also linear, quadratic or even cubic approximations of the system at some crucial frame points. This is not sufficient to make a topological classification of the behaviours, since Grobman-Hartman theorem cannot be applied in general for non isolated singularities, see [6]. Nevertheless numerical methods using continuation techniques can be used to analyze the singularities. One feature of the problem is the existence of many local optima and applications of LMI techniques are particularly important to compare the different local optima obtained using direct or indirect numerical schemes implemented in the `Bocop` and `HamPath` softwares. Hence, we believe that this article complete in many directions the results and techniques obtained in previous articles. It is a relevant step in the problem of determining the cartography of the global optima with respect to the relaxation parameters in the (ideal) contrast problem in MRI and to provide substantial improvements in existing software in MRI. Also in the context of geometric optimal control it is a significant step to handle complex 4-D problems.

REFERENCES

[1] E. Allgower & K. Georg, *Introduction to numerical continuation methods*, vol. **45** of Classics in Applied Mathematics, Soc. for Industrial and Applied Math., Philadelphia, PA, USA (2003), xxvi+388

[2] J.T. Betts *Practical methods for optimal control using nonlinear programming*, Society for Industrial and Applied Mathematics (SIAM), Philadelphia (2001)

[3] F. J. Bonnans, P. Martinon & V. Grélard. *Bocop - A collection of examples*, Technical report, INRIA (2012) RR-8053

[4] B. Bonnard, J.-B. Caillau & E. Trélat, *Second order optimality conditions in the smooth case and applications in optimal control*, ESAIM: COCV **13**, no. 2 (2007), 207–236

[5] B. Bonnard & M. Chyba, *Singular trajectories and their role in control theory*, vol **40** of Mathematics & Applications, Springer-Verlag, Berlin (2003), xvi+357

[6] B. Bonnard, M. Chyba, A. Jacquemard & J. Marriott, *Algebraic geometric classification of the singular flow in the contrast imaging problem in nuclear magnetic resonance. Mathematical Control and Related Fields-AIMS*, Special issue in the honor of Bernard Bonnard. Part II., **3** no. 4 (2013), 397–432

[7] B. Bonnard, M. Chyba & J. Marriott, *Singular Trajectories and the Contrast Imaging Problem in Nuclear Magnetic Resonance*, SIAM J. Control Optim., **51** no. 2 (2013), 1325–1349

[8] B. Bonnard, M. Claeys, O. Cots & P. Martinon, *Geometric and numerical methods in the contrast imaging problem in nuclear magnetic resonance*, Acta Appl. Math., **135** no. 1 (2014), 5–45

[9] B. Bonnard & O. Cots, *Geometric numerical methods and results in the control imaging problem in nuclear magnetic resonance*, Math. Models Methods Appl. Sci., **24** no. 1 (2012), 187–212

[10] B. Bonnard, O. Cots, S. Glaser, M. Lapert, D. Sugny & Y. Zhang, *Geometric optimal control of the contrast imaging problem in nuclear magnetic resonance*, IEEE Trans. Automat. Control, **57** no. 8 (2012), 1957–1969

[11] B. Bonnard, O. Cots, J. Rouot, T. Verron, *Working Notes on the Time Minimal Saturation of a Pair of Spins and Application in Magnetic Resonance Imaging*, http://hal.archives-ouvertes.fr/hal-01721845/

[12] B. Bonnard, J.-C. Faugère, A. Jacquemard, M. Safey El Din, T. Verron, *Determinantal sets, singularities and application to optimal control in medical imagery*, ISSAC 2016, Wilfrid Laurier University, Waterloo, Canada, 2016/07/20

[13] B. Bonnard & I. Kupka, *Théorie des singularités de l'application entrée/sortie et optimalité des trajectoires singulières dans le problème du temps minimal*, Forum Math., **5** no. 2 (1993), 111–159

[14] U. Boscain & B. Piccoli, *Optimal Syntheses for Control Systems on 2-D Manifolds*, Springer SMAI, **43** (2004)

[15] R. Bulirsch and J. Stoer, *Introduction to numerical analysis*, vol.**12** of *Texts in Applied Mathematics*, Springer-Verlag, New York, 2nd edition, 1993, xvi+744

[16] J.-B. Caillau, O. Cots & J. Gergaud, *Differential continuation for regular optimal control problems*, Optimization Methods and Software, **27** no. 2 (2011), 177–196

[17] M. Claeys, J. Daafouz, and D. Henrion. *Modal occupation measures and {LMI} relaxations for nonlinear switched systems control*, Automatica, **64** (2016), 143–154

[18] S. Conolly, D. Nishimura & A. Macovski, *Optimal control solutions to the magnetic resonance selective excitation problem*, IEEE Trans. Med. Imaging, **5** no. 2 (1986), 106–115

[19] M. Gerdts, *Optimal Control of ODEs and DAEs*, ed. De Gruyter, Berlin (2011)

[20] D. Henrion, J. B. Lasserre & J. Löfberg, *GloptiPoly 3: Moments, Optimization and Semidefinite Programming*, Optim. Methods and Software, **24** no. 4-5 (2009), 761–779

[21] A. J. Krener, *The high order maximal principle and its application to singular extremals*, SIAM J. Control Optim., **15** no. 2 (1977), 256–293

[22] I. Kupka, *Geometric theory of extremals in optimal control problems. I. The fold and Maxwell case*, Trans. Amer. Math. Soc., **299** no. 1 (1987), 225–243

[23] M. Lapert, Y. Zhang, M. Braun, S. J. Glaser & D. Sugny, *Singular extremals for the time-optimal control of dissipative spin 1/2 particles*, Phys. Rev. Lett., **104** no. 2 (2010), 083001

[24] M. Lapert, Y. Zhang, M. A. Janich, S. J. Glaser, and D. Sugny, *Exploring the physical limits of saturation contrast in magnetic resonance imaging*, Sci. Rep., **589** (2012)

[25] J.-B. Lasserre, *Moments, Positive Polynomials and Their Applications*, Imperial College Press, London (2009)

[26] J.-B. Lasserre, D. Henrion, C. Prieur, and E. Trélat. *Nonlinear optimal control via occupation measures and LMI-relaxations*, SIAM J. Control Optim., **47** no. 4 (2008), 1643–1666

[27] M. H. Levitt, *Spin dynamics: Basics of Nuclear Magnetic Resonance* John Wiley & Sons, New York-London-Sydney (2008)

[28] L. Markus, *Quadratic differential equations and non-associative algebras*, Princeton Univ. Press, Princeton, N.J. (1960), 185–213

[29] H. Maurer, *Numerical solution of singular control problems using multiple shooting techniques*, J. Optim. Theory Appl., **18** no. 2 (1976), 235–257

[30] ApS Mosek. *The mosek optimization toolbox for matlab manual*, Version 7.1 Revision 28 (2015)

[31] J. Nocedal and S. J. Wright, *Numerical optimization*, Springer-Verlag, New York (1999)

[32] L. S. Pontryagin, V. G. Boltyanskiĭ, R. V. Gamkrelidze & E. F. Mishchenko, *The Mathematical Theory of Optimal Processes*, Translated from the Russian by K. N. Trirogoff, edited by L. W. Neustadt, Interscience Publishers John Wiley & Sons, Inc., New York-London (1962)

[33] M. Putinar, *Positive polynomials on compact semi-algebraic sets*, Indiana Univ. Math. J., **42** no. 3 (1993), 969–984

[34] H. Schättler, *The local structure of time-optimal trajectories in dimension three under generic conditions*, SIAM J. Contr. Opt., **26** no. 4 (1988), 899–918

[35] H. J. Sussmann, *Time-optimal control in the plane, in Feedback control of linear and nonlinear systems*, (Bielefeld/Rome, 1981), vol. 39 of Lecture Notes in Control and Inform. Sci., Springer, Berlin (1982), 244–260

[36] H.J. Sussmann, *Regular synthesis for time-optimal control of single-input real-analytic systems in the plane*, SIAM J. Control and Opt. **25** no. 5 (1987), 1145–1162

[37] E. Van Reeth, H. Ratiney, M. Tesch, D. Grenier, O. Beuf, S. J. Glaser & D. Sugny, *Optimal control design of preparation pulses for contrast optimization in MRI*, J. Magn. Reson., **279** (2017), 39–50.

E-mail address: bernard.bonnard@u-bourgogne.fr
E-mail address: olivier.cots@irit.fr
E-mail address: jeremy.rouot@grenoble-inp.org
E-mail address: thibaut.verron@jku.at